AIAA SciTech Forum
12-16 January 2026, Orlando, FL
AIAA SCITECH 2026 Forum

10.2514/6.2026-0937

Check for updates

Mars Aerial and Ground Global Intelligent Explorer (MAGGIE): Mission Feasibility Study

Gecheng Zha [*], Yan Ren [†], Miranda Anhalzer [‡]
CoFlow Jet, LLC, Miami, Florida 33124

Michael A. Mischna [§]
Jet Propulsion Laboratory, California Institute of Technology, Pasadena, CA 91109-8099

Michael M. Sori [¶]
Purdue U., Earth, Atmospheric, and Planetary Sciences, West Lafayette, IN 47907

Downloaded by Gecheng Zha on February 9, 2026 | http://arc.aiaa.org | DOI: 10.2514/6.2026-0937

Abstract

This paper conducts a mission feasibility study for a novel global mobility Mars exploration platform: Mars Aerial and Ground Intelligent Explorer (MAGGIE). MAGGIE is a compact fixed-wing aircraft with ultra-high productivity efficiency powered by solar energy to fly in the Martian atmosphere. It has vertical take-off/landing (VTOL) capability enabled by advanced deflected slipstream CoFlow Jet (CFJ) technology. MAGGIE is designed to have a gross weight of 125 kg, payload of 20 kg, wing span of 14.12 m, and a total range of 42,011 km with level cruise for one Martian year mission. It cruises at a Mach number of 0.17 at an altitude of 1000 m with a service ceiling of 12 km. CFJ Active Flow Control (AFC) would be the enabling technology to operate in Mars' low Reynolds number ($Re < 10^5$) conditions with a very high cruise lift coefficient of $C_L = 3.24$ and aerodynamic efficiency of 5.76. Rocket launch and EDL (entry, descent, landing) for MAGGIE are feasible by using Vulcan Centaur, NASA's SLS (B2), or SpaceX Starship.

There are three types of flight trajectories for MAGGIE based on the science missions: 1) Level Cruise: cruise at 1000 m altitude for a range of 125.8 km per charge, suitable for meteorology or ice measurements; 2) Climb-and-Glide: climb to service ceiling of 12 km and then glide to ground for the longest range of 139.84 km per charge, useful for long range flight to the regions where EDL is challenging, like the southern highlands; 3) Climb-and-Spiraling Glide: climb to the service ceiling above the location of interest and then descend via spiral-glide, suitable for magnetic field measurements. All three trajectories can incorporate "scout-and-land" flight missions.

Based on the survey of the science landscape conducted in this study, a potentially ground breaking representative mission enabled by the long range and high payload capacity of MAGGIE is developed to address four atmospheric and geophysical science objectives: 1) Determine the timing of the ancient Martian core dynamo; 2) Distinguish between competing hypotheses on the distribution of mid-latitude ice on Mars; 3) Localize sources of methane emission identified on the Martian surface; 4) Characterize dynamics of the Martian lower atmosphere.

Compared with the state of the art Mars Rotorcraft Chopper, which would have a payload of 3 kg, a range of 3 km per charge (per sol) that would translate to a range of 2,000 km per Martian year, MAGGIE would span 40,000+ km areas per year with a payload of 20 kg, a cruise altitude of 1000 m, and a service ceiling of 12,000 m to perform global scale, advanced science investigations in the atmosphere and on the ground. If a conventional fixed-wing VTOL aircraft is considered for the same flight conditions as MAGGIE, a comparative assessment indicates that it would be unable to generate sufficient lift to support its own structural weight in the Martian environment, due to the inherently low achievable lift coefficient.

MAGGIE would be the first mission to enable widespread exploration of the ancient Southern Highlands of Mars and would provide a substantial leap in capability for NASA's exploration of the Red Planet. This conceptual study indicates that the MAGGIE concept and its science mission are feasible.

[*] President, NIAC Fellow, Professor of Univ. of Miami
[†] CTO, Ph.D.
[‡] Consultant
[§] Principal Scientist, Mars Exploration Program Office
[¶] Associate Professor

Copyright © 2026 by Gecheng Zha, Yan Ren, Miranda Anhalzer, Michael A. Mischna, and Michael M. Sori. Published by the American Institute of Aeronautics and Astronautics, Inc., with permission.

1 Introduction

The guideline of the NRC [1] for space exploration indicates that "mobility is not just important for solar system exploration – it is essential. The case is exemplified for Mars, where spacecraft mobility would enable major advances in understanding climate change and geologic history and in searching for direct evidence of past life". A recent report by the Mars Concurrent Exploration Science Analysis Group (MCE-SAG) [2], chartered by NASA's Mars Exploration Program (MEP), has established a set of high-priority science objectives to be pursued in parallel with NASA's Mars Sample Return program under the theme of "Dynamic Mars: Investigating ancient and modern drivers of change on an active planet." Timescales cover both long term (billion-year) and short term (diurnal) change and reflect the ongoing processes that have evolved Mars from what was once a much different, potentially Earth-like environment into the present cold, dry desert. In support of this science are several program initiatives to be pursued in the coming decades, including "advancement of capabilities in aerial mobility, surface mobility and autonomy" [3].

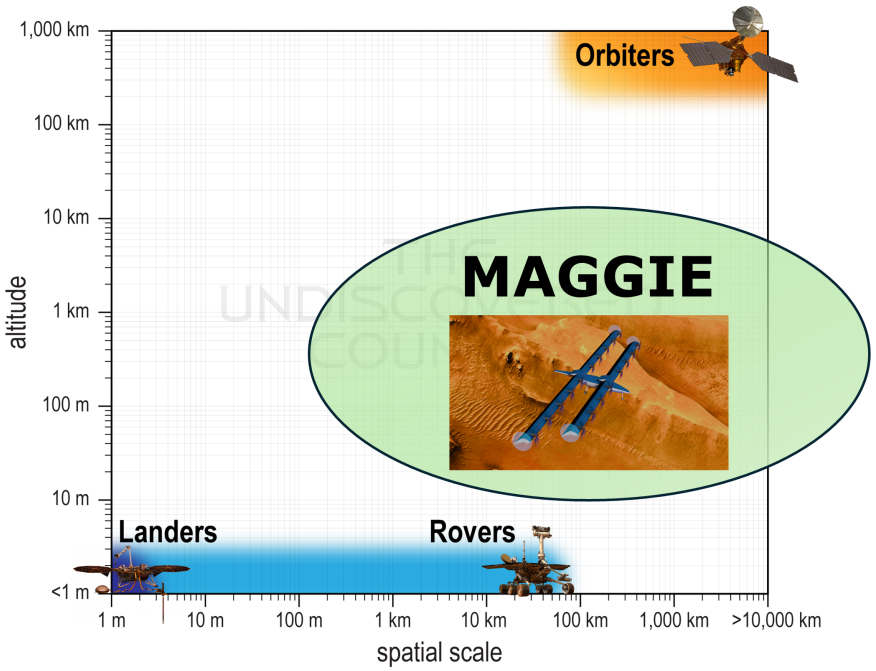

Fig. 1: Range and altitude for different Mars explorers.

At present, Mars science is accomplished through orbiters (e.g., the Mars Reconnaissance Orbiter), rovers (e.g., Perseverance), or stationary landers (e.g., InSight). Abundant scientific discoveries have been made from these past missions, but large knowledge gaps remain that require data that can only be acquired from new mission architectures. Orbiters generally provide data globally from high altitudes at comparatively low resolution, while rovers and landers provide high-resolution ground truth but at only one or a few locations on the surface. Current technology for aerial vehicles provides no real advantage in spatial coverage over landers in this context. To bridge the gap between rovers and orbiters, an aerial vehicle that can land anywhere on Mars with a global-scale range and provide an orders of magnitude higher-resolution survey than orbiters from a kilometers altitude is appealing. The novel aerial concept, Mars Aerial and Ground Global Intelligent Explorer (MAGGIE) is to serve this purpose. Fig. 1 shows the comparison of the spatial and altitude scales of different explorers. MAGGIE, with its global-scale range of more than 40,000 km and altitude 1-12 km fills the important blank space between ground rovers and high altitude orbiters.

The recent great success of the solar-powered Ingenuity helicopter opens an era of aircraft flying on Mars. Even though Ingenuity is mostly a demonstrator of flight feasibility on Mars with an endurance

Downloaded by Gecheng Zha on February 9, 2026 | http://arc.aiaa.org | DOI: 10.2514/6.2026-0937

less than 3 min per flight, total mass of only 1.8 kg, and almost no payload, it has inspired a vision of developing Martian aircraft as global-scale explorers both near to, and on, the Martian surface.

To address high-priority scientific questions on the global scale, at, and near, the Martian surface requires an aircraft with the following features: 1) vertical takeoff and landing (VTOL) capability to examine the atmosphere and surface at any place on Mars; 2) low weight, high efficiency, and with a long range and large payload mass for scientific equipment; 3) sustainability and self-sufficiency in energy. The first two features depend on the aircraft aerodynamic performance and are seriously limited by the low density of the Martian atmosphere. For the third feature of energy self-sufficiency, solar energy is ideal since it can be generated anywhere on Mars when the Sun is up. But the solar energy on Mars is only about 44% of that on Earth due to its greater distance from Sun. All these limitations make designing a global-scale aircraft on Mars extremely challenging using conventional aerodynamic technologies.

1.1 Overview of Possible Mars Aircraft Configurations

NASA has conducted intensive studies on various Martian aircraft configurations in the past seven decades as summarized by Guynn et al. [4] for their work on the ARES concept (Aerial Regional-scale Environmental Survey of Mars) [4–7]. ARES made it to Step 2 of the 2002 Mars Scout mission call. Their conclusion was that a powered aircraft is most desirable to perform controlled aerial science missions.

However, there are several challenges to designing a Martian aircraft. "The first and foremost consideration in Mars airplane design is the nature of the Martian atmosphere." as pointed out by the ARES team [4]. The Martian atmosphere has a low density of about 1% that on Earth. The low air density yields very low wing loading and a low Reynolds number for flying on Mars. The Martian gravity of about 1/3 of that on Earth only increases the equivalent air density from 1% to 3% of that on Earth, hardly helpful. Conventional aerodynamic technology has few techniques to counter the effect of low density. This is because the suitable cruise lift coefficient of subsonic aircraft is 0.3-0.6 in order to have high efficiency and sufficient stall margin. Such a lift coefficient, which has remained little changed for decades since WWII, is too low to balance the low air density on Mars. The low lift coefficient affects both fixed wing aircraft and helicopter blades for flying on Mars. Furthermore, the low Reynolds number for flying on Mars exacerbates the already very poor flow conditions with reduced aerodynamic efficiency, lift coefficient, and operating range due to the flow prone to separation and stall [4, 8].

Scaled-up Ingenuity-type helicopters such as the Mars Rotorcraft Chopper [9] evolved from the 'Mars Science Helicopter' (MSH) concept [10] are considered as potential aerial vehicles for Mars science mission exploration. However, helicopters have substantially lower cruise efficiencies than fixed-wing aircraft for a given range and payload. Ingenuity installed its solar panel above the propeller because it is not desirable to put solar panels on the rotating propeller blades due to high centrifugal load. Such a configuration may be difficult to scale up due to interference with the flow (e.g., downwash) passing the rotor at hover and forward flight [11]. The solar panel configuration would further penalize the low mission efficiency of helicopters, making the Chopper or MSH concepts more suitable for small range (e.g., less than 10 km per flight) exploration instead of a global range with a significant payload.

A fixed-wing VTOL aircraft is more efficient aerodynamically for flying for a long range and with a large payload. For energy self-efficiency, an important advantage of a fixed-wing aircraft is that it can integrate solar panels within its wings and fuselage to be aerodynamically and structurally efficient. However, the low wing loading of a conventional fixed-wing aircraft like that previously mentioned would be very difficult to fly on Mars while maintaining significant range and payload. It would require a very large wing surface with a correspondingly heavy weight. It would have to fly fast to avoid an excessive wing size. For example, ARES [4–7] was designed to fly at Mach 0.65 powered by a rocket engine. Such a high speed is feasible for a "one-shot" flight but is insurmountable for achieving energy self-sufficiency and performing global-scale scientific investigations using solar power on Mars. This is because the energy required is proportional to the square of the flight speed for a fixed distance and the power required is proportional to the cube of the flight speed. The propulsion system weight is proportional to

Downloaded by Gecheng Zha on February 9, 2026 | http://arc.aiaa.org | DOI: 10.2514/6.2026-0937

the maximum power required. The low wing loading, large size and weight, and high power and energy required based on conventional technology render a fixed-wing electric VTOL (eVTOL) Martian aircraft powered by solar energy as infeasible for achieving global-scale range with a useful science payload.

Other potentially useful airborne systems for Mars exploration include balloons or aerobots [12], which either use gases lighter than the ambient atmosphere or heat the enclosed ambient atmosphere gas. Balloons share some of the advantages of Martian aircraft; however, they have some serious disadvantages: 1) the payload is very limited due to the thin atmosphere on Mars; 2) it is very difficult to control navigation, deployment, altitude changes, and landing in the Mars environment due to the large size of the balloons [12].

To achieve a fixed-wing eVTOL aircraft for global-scale Mars science exploration, an advanced, beyond the current state-of-the-art aerodynamic technology that would approach nearly an order of magnitude higher cruise lift coefficient and mission productivity efficiency is crucial. This research investigates the essential steps of MAGGIE's flight envelope and indicates the concept is feasible.

2 Feasibility Study Process

The feasibility study is an iterative process with multidisciplinary design optimization as illustrated in Fig. 2 among three missions: 1) MAGGIE's flight mission on Mars, 2) science representative mission; 3) launch mission from Earth to Mars. Each box represents a task studied. Primary efforts are focused on the MAGGIE vehicle flight mission on Mars (blue boxes) needed to satisfy the requirements of the science representative mission.

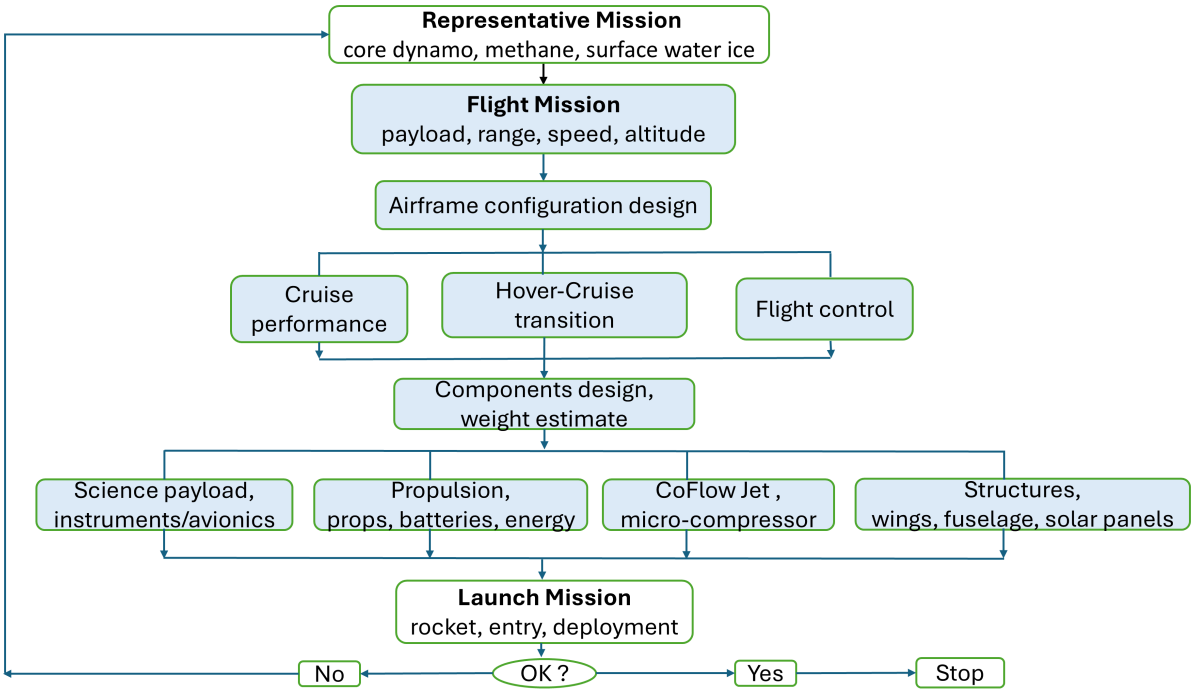

Fig. 2: Feasibility study process and conceptual design of MAGGIE's missions.

3 Numerical Approaches

The in-house high-order-accuracy CFD code FASIP (Flow Acoustics Structure Interaction Package) developed under the support of AFOSR, NASA, DARPA, GUIde, NSF [13–28] is used for all the CFD simulations of the CFJ systems and full aircraft configurations. FASIP solves the full 3D time dependent Navier-Stokes equations in generalized coordinates using multi-block structured meshes that can treat complex geometries. For the inviscid fluxes, FASIP employs 3rd and 5th order WENO shock-capturing schemes with a low diffusion approximate Riemann solver of Roe [29] or the E-SUMP scheme of Zha et al. [20]. It uses 2nd, 4th, and 6th order central differencing schemes for the viscous terms. For unsteady flow simulation, FASIP adopts a 2nd order time accuracy and implicit time

Downloaded by Gecheng Zha on February 9, 2026 | http://arc.aiaa.org | DOI: 10.2514/6.2026-0937

marching scheme implemented with unfactored line Gauss-Seidel iteration [30]. FASIP can simulate laminar flows and turbulent flows with various advanced turbulence models, including the model of Spalart-Allmaras (SA), SST, IDDES, and LES. The code is extensively validated with various CFJ airfoil flows, 2D, 3D, steady/unsteady simulations, fluid-structural interaction, and turbomachinery flows [21, 22, 24–28, 31–40]. The code has high scalability efficiency parallel computing using MPI [41].

3.1 Validation with Low Reynolds Number

The numerical strategy developed by Koning et al. [42, 43] and Winslow et al. [44] to simulate the flows of low Reynolds numbers ($Re < 10^5$) using a time accurate SA full turbulence model is adopted in our study. Their results are validated well with experiments. Koning et al. [42] quote the discussion of Rumsey and Spalart [45] on the use of the SA turbulence model at low Reynolds numbers, "at low Reynolds numbers it is likely that the turbulence models will not become activated over much of the airfoil surface, and the higher the Mach number, the larger the laminar region is likely to be. It is observed that the fully turbulent SA model produces almost identical results to the fully laminar solver in the linear angle of attack (AoA) range before airfoil stall [42, 43], which was the range of our interest in this feasibility study.

For the low Reynolds number flow cases, we have validated multiple cases [46], including a triangular airfoil at $M = 0.15$ and Re =3,000 with experiment and the CFD results of Koning et al. [47] using the SA model and the results of Munday et al. [48] using direct numerical simulations (DNS). Our validations agree very well with the experiment and the CFD results of [47, 48]. For brevity, we only show one low Reynolds number flow validation case below.

The validation case presented here compares our FASIP with the experiment and the CFD results in [44] for a NACA0009 airfoil at a Reynolds number of 50,000 and Mach number of 0.1. This case has the Reynolds number and Mach number in the same range as in our MAGGIE design. Fig. 3 and 4 show that FASIP predicts the lift coefficient (C_L) and drag coefficient (C_D) in very good agreement with the experiment and the results [44] in the linear angle of attack (AoA) range from 0° to 7°. Fig. 5 shows that the upper surface pressure distributions predicted by the FASIP code at an AoA of 0°, 3°, and 5° also agree very well with the experiment and the results [44]. Starting at an AoA of 8°, the flow has trailing edge separation as shown in Fig. 6. The experiment shows the airfoil starts stalling. Both numerical results predict the stalling point (AoA) fairly well, but the C_L quantitative value deviates from the experiment as expected due to the inadequacy of the turbulence model. As long as the flow is in the linear region with attached flow, which is our focus, FASIP predicts the low Reynolds number flow results very well.

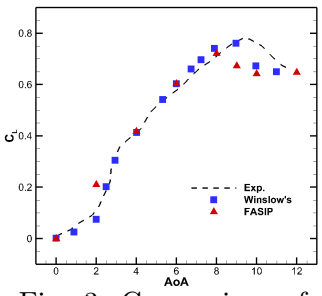

Fig. 3: Comparison of C_L for NACA0009 airfoil

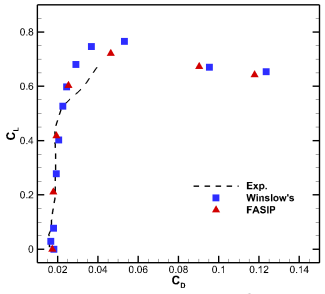

Fig. 4: *Dragpolar*

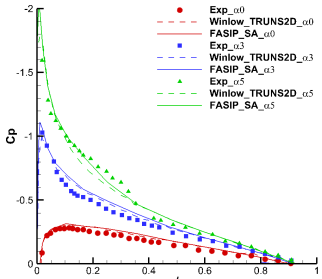

Fig. 5: Surface pressure coefficient on upper surface of NACA0009 airfoil

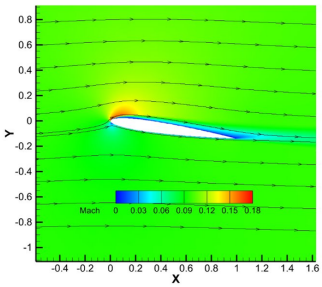

Fig. 6: Mach contour NACA0009 airfoil at AoA 8°

4 MAGGIE's Configuration

MAGGIE is a tailless VTOL aircraft with a long wing in the rear and a canard in the front cruising at Mach number 0.17 (41.2 m/s) at an altitude of 1000 m. Fig. 7 and Fig. 8 show MAGGIE's configuration at cruise and hover. More geometry and mission info is given in Table 1. The VTOL configuration is designed based on an innovative aerodynamic concept of deflected slipstream (DS) enabled by a flapped

Downloaded by Gecheng Zha on February 9, 2026 | http://arc.aiaa.org | DOI: 10.2514/6.2026-0937

CFJ airfoil [49–51], which has a micro-compressor actuator (MCA) pumping system embedded inside the flap as shown in Fig. 8 and 9. The MCA sucks a small amount of air mass flow near the trailing edge, pressurizes it, and ejects the air as a jet at the flap shoulder tangent to the surface.

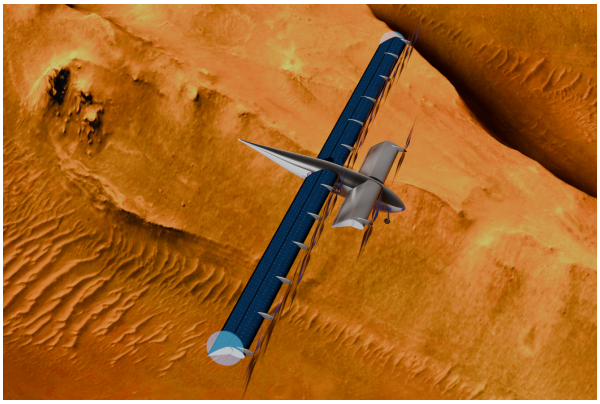

Fig. 7: MAGGIE at cruise.

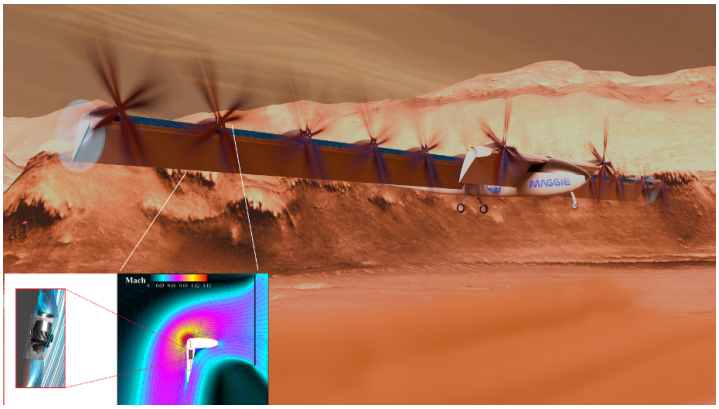

Fig. 8: MAGGIE at VTOL hover enabled by DS-CFJ with MCAs embedded inside the flap.

Fig. 9 shows the thick-flapped CFJ-NACA-6421 airfoil used for MAGGIE, which utilizes a simple hinge to control the plain CFJ flap that has a length of 60% chord. At hover, the flap turns the slipstream from the propellers 90° downward by deflecting the flap 75° as shown in Fig. 10 for 2D and Fig. 11 for 3D simulations. Based on aerodynamics momentum theory, a 90° flow turning converts all the thrust of the propellers to vertical lift for takeoff and landing. Fig. 12 shows recent testing funded by NASA LaRC to demonstrate that the deflected slipstream can be turned 90° by the CFJ flap deflected 78° at static condition on Earth [49]. Such a feature enables MAGGIE to take off and land vertically without tilting the rotors or the wings, substantially simplifying the system, reducing the weight, and increasing reliability. However, deflecting the slipstream 90° downward is not feasible using conventional flap systems, including slotted flaps [52–54]. For cruise, the flap deflection angle, β, will be reduced to 35° as shown for the rear wing in Fig. 14 since the lift coefficient required would be lower. Fig. 14 is a cross section at the canard mid-span from the 3D results of Fig. 13. The tandem wing configuration is designed using tip vortex capturing technique suggested by Ren and Zha [55, 56].

For flight control, the flap on each side of the wing will have multiple segments along the span to provide effective pitching and rolling control. For yaw control, a total of 14 propellers and 36 MCAs embedded inside the flaps are control actuators together with the flaps [57, 58]. The large number of propellers and MCAs also provide high redundancy to increase the operation reliability.

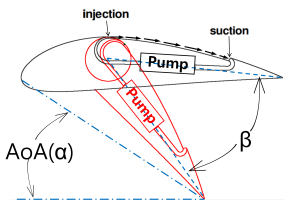

Fig. 9: Flapped CFJ airfoil.

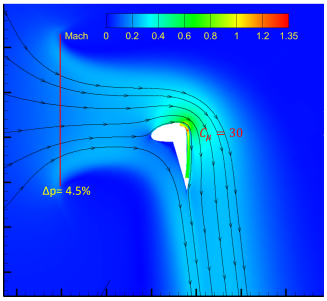

Fig. 10: DS-CFJ airfoil deflecting slipstream 90° at hover.

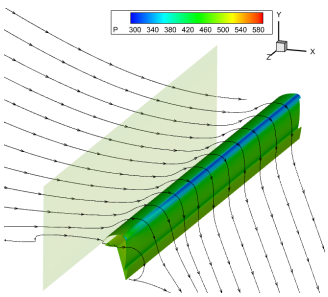

Fig. 11: Computed 3D CFJ-DS turning flow 90°.

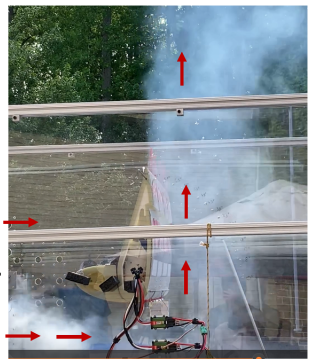

Fig. 12: Flow visualization in testing.

Downloaded by Gecheng Zha on February 9, 2026 | http://arc.aiaa.org | DOI: 10.2514/6.2026-0937

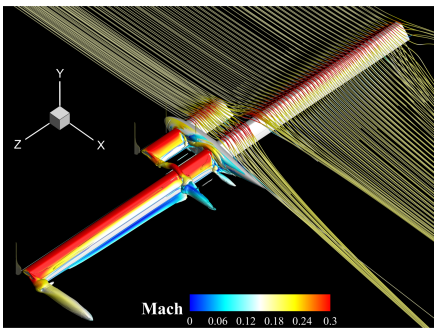

Fig. 13: CFD simulated MAGGIE at cruise [55].

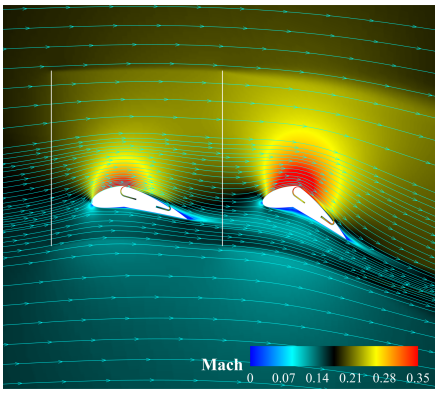

Fig. 14: Mid-span of the canard at cruise [55].

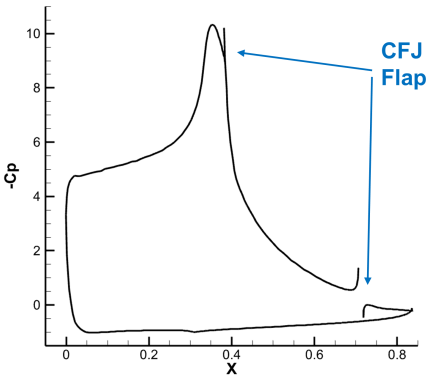

Fig. 15: Cp distribution at mid-span [55].

Downloaded by Gecheng Zha on February 9, 2026 | http://arc.aiaa.org | DOI: 10.2514/6.2026-0937

5 Aerodynamics Physics

The physics mechanism by which a thick-flapped CFJ airfoil can resist flow separation at low Reynolds number and generate an ultra-high lift coefficient, C_L, and aerodynamic efficiency, $C_L/(C_D+P_c)$ (where C_D is the drag coefficient; P_c is the power coefficient), can be explained by the following three factors:

1) The flapped CFJ airfoil has a surface pressure coefficient, Cp, distribution very different from a conventional one with significant advantages. Fig. 15 shows the Cp distribution at the mid-span section of the 3D wing from Fig. 13 at cruise condition with a C_L of 3.24 [55]. The thick and round front part of the flapped CFJ airfoil geometry greatly opens up the Cp distribution, contributing a majority of the high lift coefficient. An important advantage of the major lift generated in the front part of the airfoil is that the flow is in a favorable pressure gradient (FPG) in this region until it reaches the suction peak at the shoulder of the flap at about the 40% chord position. Flow naturally remains attached in a FPG region. The largest adverse pressure gradient (APG) occurs downstream of the suction peak on the airfoil flap, where the coflow jet also occurs as indicated in Fig. 15. The CFJ energizes the boundary layer and keeps the flow attached. This is the most critical part. Without the flow attached on the flap, the whole pressure distribution will collapse without the front part contributing a majority of the lift coefficient. The large acceleration at the airfoil leading edge decreases the pressure there, thus reducing the pressure drag and overall drag [32, 59, 60].

For a conventional airfoil, the pressure coefficient distributions on the upper surface of a NACA0009 airfoil as shown in Fig. 5 are typical, and are clearly very different. It has the suction peak value much lower than that of the flapped CFJ airfoil and the suction peak is also located at the very leading edge. It almost has the entire upper surface in APG, which makes low Reynolds number airfoil flow prone to separation and stall at a low AoA of 8°. Thin airfoils with thickness less than 6% are therefore more desirable [44, 61, 62]. For the Mars Science Helicopter, an airfoil with 1% thickness is used for the propellers [62]. However, such a thin airfoil would be very difficult for use on a fixed wing VTOL aircraft due to its weak structural strength and increased weight, which is inversely proportional to the thickness to the power of 0.3 [63], since a thin wing needs to use stronger or more material to sustain the load.

2) The injection jet interacts with the main flow at the shoulder of the flap and forces the boundary layer to transition to turbulent in the APG region on the flap, and makes the flow stay attached. Even though the Reynolds number based on the airfoil chord is low under Mars conditions, the injection jet Reynolds number based on the slot height is about 3500, which makes the jet fully turbulent. CFJ is shown to be able to attach the flow at AoA of 65°, overcoming extreme APG (EAPG) 700x greater than that which the conventional airfoil counterpart can sustain without flow separation due to largely enhanced turbulence diffusion [64–67]. Fig. 10 shows the flow is attached at an AoA of 55° at low Re, providing MAGGIE a much larger stall margin than conventional airfoil that would stall below AoA of

15° at low *Re* (see Fig. 3). Immersing the CFJ in the entire APG region like the one shown in Fig. 15 is the most efficient and effective way to resist EAPG [68, 69].

3) To achieve a high aerodynamic efficiency $C_L/(C_D + P_c)$, not only do a high C_L and low C_D need to be achieved, but the power coefficient of CFJ, P_c, must also be low. The CFJ injection is at the shoulder, which has the lowest main flow pressure as shown in Fig. 15 and thus requires a low power to eject the flow out. The suction is near the trailing edge, which has nearly the highest pressure in the main flow and thus requires a low power to suck the flow in. The unique injection and suction mechanism with zero-net-mass-flux makes CFJ achieve a high lift coefficient, low drag coefficient, and very low energy expenditure, resulting a high aerodynamic efficiency.

6 MAGGIE's Flight Mission

Table 1 gives some MAGGIE geometry parameters and flight mission performance metrics based on CFD simulation and eVTOL aircraft mission design [70–73]. The wing chord is 0.7 m. The rear wing has a circular tip cap installed that increases the aerodynamic efficiency by about 6.6% compared with the wing without the tip cap [74]. MAGGIE's service ceiling, the highest altitude that it can fly, is 12 km. Such high altitude is valuable for studying the Martian atmospheric boundary layer and magnetic field to be described in Section 10.

The design as shown in Fig. 13 achieves the targeted lift coefficient, C_L, of 3.24 and productivity efficiency of $C_L^2/(C_D + P_c) = 18.72$. Such a lift coefficient is nearly an order of magnitude higher than a conventional aircraft at low Reynolds numbers with the same configuration as to be shown in Section 9. MAGGIE's configuration is designed using the vortex-capturing strategy we developed [73] to enhance the overall wing system efficiency.

The power density of the micro-compressor used to estimate the weight is 3 kW/kg, a very achievable performance based on the state-of-the art in industry. The designed micro-compressor efficiency is 70%. In our mission analysis, an efficiency of 65% at cruise and 60% at hover is used to account for some extra loss.

The co-axial counter-rotating propeller configuration with blade pitching developed for MSH [62, 75] is adopted for all the propellers. Blade feathering feature will be implemented with the variable pitch system since MAGGIE would perform spiral glide or linear glide. A measure of merit of 67% achieved in [62] is also used in this design. The dust on Mars is mostly micron-sized particles and can smoothly pass through the CFJ airfoil slots and micro-compressors blades that are on the order of 10 mm. However, the CFJ also has a debris filtering system to discard any heavier-than-air debris (e.g., dust, sand) with centrifugal force at the suction duct turning [76]. The propellers and CFJ blowing on the upper surface are also beneficial for removing dust deposits on the wing with solar panels.

Performance	Value
Cruise Mach number	0.17
Altitude, cruise (m)	1000.00
Service ceiling, km	12.00
Range/Martian day (km)	61.22
Range/Martian Year (km), Level cruise	42011.11
Range/charge (km), level cruise	125.76
Range/charge (km), Service ceiling glide	139.84
Glide angle, deg	9.58
Cruise time/charge (h)	0.85
Battery charge time (Martian day)	2.05
Solar panel energy/Martian day (kwh/m^2)	0.43
Cruise speed (m/s)	41.20
Power cruise (kw)	5.07
Power, hover (kw)	50.70
Max power/prop, kw	1.93
Total mission available energy (kwh)	6.97
Total mission required energy (kwh)	4.88
Service ceiling, km	12.00
Battery energy reserved+discharge loss, %	0.30
Energy used for heating per night (kwh)	0.09
Battery enegy density, WH/kg	300.00
Power density of Micro-compressor (kw/kg)	3.00
Number of Micro-comprssors	36
CL, cruise	3.24
CL/CD	11.18
CL/CDc = CL/(CD+PC)	5.76
Aspect Ratio	17.35
Solar panel area (m^2)	5.50
Fuselage width (m)	0.49
Aircraft length (m)	4.00
Wing span, front (m)	3.62
Wing span, rear (m)	14.12
Chord (m)	0.70
Wing Area (m^2)	12.25
Diameter, prop front (m)	1.26
Number of front props	2
Diameter, prop rear (m)	1.23
Number of rear props	12

Table 1: MAGGIE performance

For the solar energy estimate, instead of using a constant solar cell power density of 540 $\mathrm{Wh/m^2/sol}$ as adopted in the MSH design [62], a linear degradation by 40% at the end of the one year mission is utilized. The solar panels are only put on the rear wing of MAGGIE with a total area of 5.5 $\mathrm{m^2}$, which is sufficient to fly for an average range of 61.22 km per sol. An energy storage system of Li-ion batteries

Downloaded by Gecheng Zha on February 9, 2026 | http://arc.aiaa.org | DOI: 10.2514/6.2026-0937

is used with an energy density of 300 Wh/kg, which is currently available based on the announced cell level of 450-500 Wh/kg by Amprius and CATL on their company websites. The flight range is achieved by using only 70% of the total battery energy with 20% reserved energy and 10% energy loss. The sleep energy, which is to keep the science instruments and propulsion system at the operating temperature at night, is calculated using the model based on the gross weight [62] with a battery efficiency of 85%.

MAGGIE has a gross mass of 125 kg based on estimates using empirical correlations and calibrated data from Ingenuity in the MSH study [62]. Table 2 has the weight breakdowns for all its components. The structure will be made based on the similar carbon composite material used for the blades of the Ingenuity Mars helicopter. The weight of the wings is estimated using the scaling correlation for aircraft wing [63] that includes the effect of planform area, airfoil thickness, load factor, gross weight, aspect ratio, sweep angle, taper ratio, etc. The mass of the Ingenuity blades is used as the reference for weight scaling [62, 75]. The large airfoil thickness of MAGGIE does bring significant benefit for weight reduction [63]. The weight estimate is more on the conservative side since the wing does not have a centrifugal load like the helicopter blades and the dimensions are also much larger, which gives a greater load limit per unit area. The weight of the fuselage and landing gears is also based on the correlations given in [63], but for atmosphere and gravitational acceleration conditions on Mars. The weight of the propellers and the motors are estimated assuming the same power density for the propulsion components of MSH [62]. The solar panel contributes a significant part of the total weight with a density of 2 kg/m^2 [62, 75]. Overall, the weight estimate is more on the conservative side and also has a contingency margin of 7.7 kg to manipulate for unexpected usage.

Component	Mass (kg)
Wing	17.64
Fuselage	5.45
Landing gear	3.12
Payload (Instruments)	20.00
Micro-compressors	7.92
Solar panel	11.00
Battery	23.24
Avionics	1.00
Propulsor system	34.60
Contigency	1.00
Gross Mass	124.96

Table 2: Mass of MAGGIE's components.

6.1 Flight Trajectories

The MAGGIE aerial vehicle, after an initial vertical takeoff and ascent to 1000 m altitude, can execute three primary flight trajectories, as illustrated in Fig. 16 (not to scale):

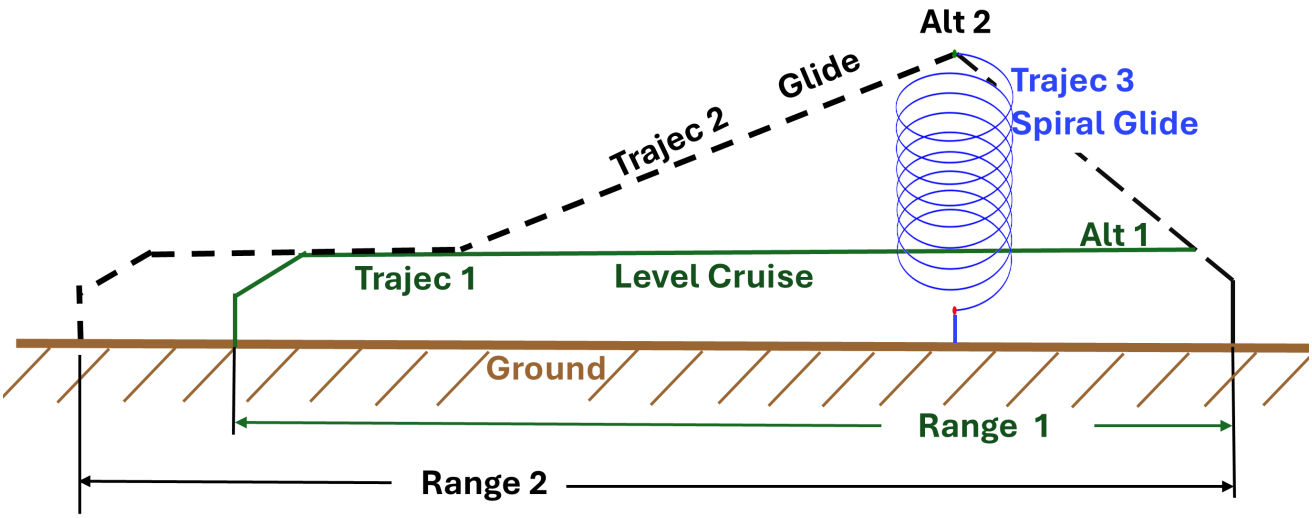

Fig. 16: Sketch of the three MAGGIE flight trajectories (not to scale).

1) Level Cruise (Fig. 16, Trajec 1 in green): Vertically takeoff and transition to cruise at a constant altitude of 1000 m (Alt 1) at speed of 41.2 m/s (Table 1) for flight missions such as meteorology or ice measurements. This trajectory provides a range of 125.76 km per charge and is suitable for meteorology

Downloaded by Gecheng Zha on February 9, 2026 | http://arc.aiaa.org | DOI: 10.2514/6.2026-0937

or ice measurements. The designed total range of 42,011 km per Martian year in Table 1 is based on this level cruise profile.

2) Climb-and-Glide (Fig. 16, Trajec 2 in black): First vertically takeoff and climb to the 12 km service ceiling (Alt 2) (Table 1) at a constant speed, then glide and descend to the altitude of 1000 m before entering a level cruise until the flight mission reserved energy is depleted. This trajectory yields the longest range of 139.84 km per charge, which would be useful for enabling access to regions of Mars where EDL is challenging, like the southern highlands.

3) Climb-and-Spiraling Glide (Fig. 16, Trajec 3 in blue): First climb to the 12 km service ceiling as Trajec 2 above the location of interest, and then descend via spiral-glide around the same location in circles with a 0.05 - 5 km radius, suitable for magnetic field measurements.

All three trajectories can incorporate "scout-and-land" flight missions if any sites of interest are discovered during flight. The climb-and-glide trajectory is detailed further below, as it requires a little more complex flight dynamics design than the level cruise.

For unaccelerated climbing,

$$L = Wcos(\theta) \tag{1}$$

$$P_{climb} = TV = WVsin(\theta) + DV + P_{CFJ} \tag{2}$$

where L is the lift, W the gross weight, θ the climb angle, P_{climb} the climb power. The drag, $D = 0.5 * \rho V^2 S C_D$, and power required for CFJ, $P_{CFJ} = 0.5 * \rho V^3 S P_c$, will vary with altitude due to air density variation.

Eq. (2) can be also expressed as

$$\frac{TV - DV - P_{CFJ}}{W} = Vsin(\theta), \quad or \quad \frac{excess\ power}{W} = Vsin(\theta) \tag{3}$$

The atmospheric density variation with altitude is determined by the Martian atmospheric model given by NASA described below (https://www.grc.nasa.gov/www/k-12/airplane/atmosmrm.html):

For $h > 7000m$

$$T(^\circ C) = -23.4 - 0.00222h \tag{4}$$

$$p(kPa) = 0.699e^{-0.00009h} \tag{5}$$

For $h < 7000m$

$$T(^\circ C) = -31 - 0.000998h \tag{6}$$

$$p(kPa) = 0.699e^{-0.00009h} \tag{7}$$

$$\rho = p/(0.1921(T + 273.1)) \tag{8}$$

For the same altitude change, the density variation on Mars is less than that on Earth.

The designed climb angle, θ, is 60° and the speed is the same as the level cruise speed of 41.2 m/s (Table 1). At such a climbing angle, the aerodynamic lift only needs to overcome half of the gross weight as shown by Eq. 1. The propulsion thrust supports the rest of the weight. The aerodynamic drag and CFJ power required are also smaller than that at cruise due to lower lift and density at high altitude. Since MAGGIE uses electric propulsion, the power available decreases little with the increasing altitude. It thus provides sufficient excess power, and the climbing power dictated by Eq. (2) and (3).

Once MAGGIE reaches the service ceiling, it will not perform level unaccelerated flight, but will start descending by low power glide to altitude of 1000 m at the speed of 41.2 m/s, complete a last leg of level unaccelerated cruise, and then conduct the final vertical landing. For gliding, the propellers will be in idle unpowered state with the rotor blades feathering to minimize the drag, but CFJ will be in full power as in level cruise to maintain the required lift coefficient. The gliding angle is 9.58° determined by C_L/C_D. Even though blade feathering would minimize the aircraft drag increase at

Downloaded by Gecheng Zha on February 9, 2026 | http://arc.aiaa.org | DOI: 10.2514/6.2026-0937

gliding, typically no more than 15%, a conservative drag increase of 100% is used for MAGGIE since it has multiple propellers. Since gliding consumes less power and the air density is also lower at high altitude, the overall range per charge for the Climb-and-Glide trajectory is about 11.2% longer than that of Level Cruise at altitude of 1000 m as shown in Table 1. Climbing to the service ceiling only takes about 5.5 minutes, but consumes about 39% of the total energy reserved for cruise. The glide takes about 26. 7 minutes, consumes about 12.29% of the total cruise energy, and contributes 50.7% of the total range. The Climb-and-Spiraling Glide trajectory is also a low power glide similar to the Climb-and-Glide trajectory.

To achieve a high service ceiling, an aircraft requires not only sufficient excess power at that altitude but also the necessary energy for climbing to the altitude. While the latter is rarely a constraint for conventional aircraft on Earth (given their large fuel capacity), it is a critical trade-off in the MAGGIE design phase. A careful balance must be struck between the weight of the batteries (which store energy) and the weight of the solar panels (which charge the batteries). The results in Table 2 indicate that MAGGIE's battery weight is slightly more than double the solar panel weight. Consequently, the aircraft requires two sols to fully charge the batteries (Table 1).

6.2 Hover-Cruise Transition

The most critical phase of a fixed wing VTOL aircraft is the transition between hover and cruise. It is particularly important to demonstrate the feasibility in Mars' low atmospheric density environment. Two essential performance features that need to be confirmed are: 1) The flapped CFJ wing will deflect the slipstream by 90° to generate sufficient hover lift with manageable power in the Martian low density static condition. 2) The transient hover-cruise transition can be controlled automatically in Mars' low density atmosphere for this new aerodynamic technology.

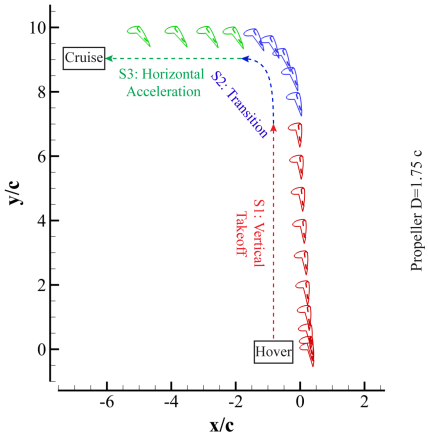

Fig. 17: Simulated flight trajectory of the DS-CFJ airfoil with 3 segments

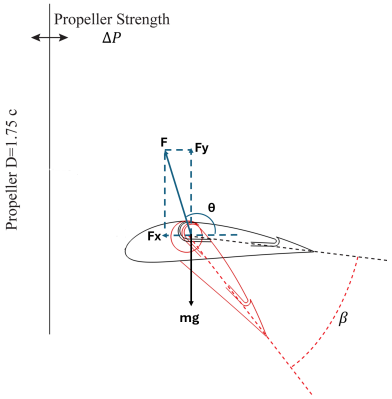

Fig. 18: DS-CFJ NACA 6421 Airfoil at transition control.

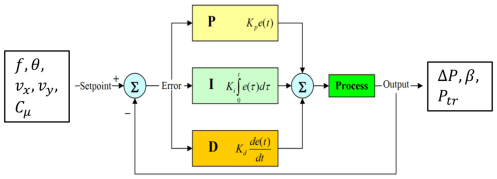

Fig. 19: PID control system for managing flight parameters.

To demonstrate the first performance feature, 2D flapped airfoil design optimization is conducted first at hover condition on Mars to sustain the weight with initial acceleration for vertical takeoff and landing as shown in Fig. 10. The same CFJ airfoil is then used to simulate the 3D hover at static condition as demonstrated in Fig. 11. Hover time with the total lift of 1.18 W is reserved for 30 s for both takeoff and landing, which is very conservative. The climbing/descending time is about 35 s.

To demonstrate the second performance feature for hover-cruise transition, automatic control, a CFD algorithm with fully coupled fluid-body interaction (FBI) of 6-degrees of freedom managed by a proportional-integral-derivative (PID) automatic control algorithm is developed in this study [77]. Due to time and resource constraints, the FBI was only simulated for 2D transition from hover to cruise in this study to demonstrate the control feasibility. 3D simulation of flight control in transition will be conducted in the next step.

Downloaded by Gecheng Zha on February 9, 2026 | http://arc.aiaa.org | DOI: 10.2514/6.2026-0937

The transition trajectory encompasses three distinct segments as depicted in Fig. 17: vertical takeoff with hover and acceleration (S1), transition from vertical motion to horizontal motion (S2), and horizontal acceleration (S3). In S1, the airfoil starts with a zero vertical velocity and ascends vertically, achieving the desired altitude. During S2, the transition segment, the airfoil maneuvers from a vertical climb to a horizontal flight. S3 represents the horizontal acceleration phase, where the airfoil continues to accelerate horizontally to reach the desired cruise speed. Fig. 18 shows the resultant force, the flap angle, and propeller strength as some of the control parameters. The control algorithm manages the flap angle (β), propeller strength (ΔP), and micro-compressor momentum coefficient (C_μ) to maintain stability and achieve the desired flight trajectory governed by the magnitude and direction of the resultant force vector, $\mathbf{f}$, and the moment. Fig. 19 shows the PID closed control loop, functions, input and output [77].

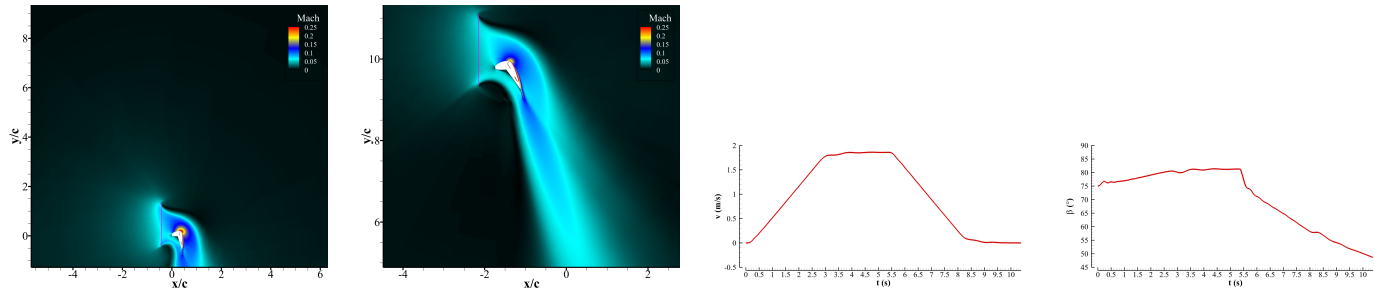

(a) $t = 0.538\,\mathrm{s}$ (b) $t = 8.065\,\mathrm{s}$ (c)v-velocity (d) β

Fig. 20: Hover-cruise transition from segment I to III: (a) and (b): Mach contours around the DS-CFJ airfoil; (c) and (d): controlled vertical velocity and flap angle.

Fig. 20 (a) and (b) show two flow field instants at the initial ascending acceleration and transition to horizontal cruise indicated by the x-, and y-coordinates with different flap angles. Fig. 20 (c) shows a smooth transition of the vertical velocity starting with acceleration from initial static velocity, ascending at constant vertical velocity, decelerating at transition to horizontal flight, and finally vanishing at the last stage at horizontal cruise. Fig. 20 (d) shows the flap angle variation from hover to cruise to achieve the transitional motion and stability.

This research result indicates that the flapped CFJ airfoil can be automatically controlled to provide stability for the hover-cruise transition. Conceptually, if 2D is feasible, then 3D is feasible with some expected efficiency penalty. The next step of the research will be conducting the 3D full aircraft configuration hover-cruise transition simulation to further confirm the feasibility.

7 Micro-compressor Actuator Design

In this study, we have conducted a design of a micro-compressor actuator in Mars' low Reynolds number environment based on our previous experience [60, 78–83]. It meets the dimensions of the CFJ-NACA6421 airfoil, required mass flow rate and pressure ratio dictated by MAGGIE's flight envelope on Mars. This is a crucial component to enable the CFJ function in Mars' atmospheric conditions. Table 3 provides the geometric and operational parameters at the design point, which corresponds to the cruise condition of MAGGIE, indicating that a very good efficiency of 70% is achieved at an RPM of 85,000. Further efficiency improvements will be assessed in the future.

Fig. 21 shows the Mach contours near the blade tip at the design point, indicating the flow is supersonic in the tip region. Fig. 22 is the MCA performance map showing the total pressure ratio mass flow rate at different RPM. The peak efficiency point at the design RPM of 85k has the mass flow, total pressure ratio and efficiency nicely matching the required conditions of MAGGIE at cruise. For hover condition, the speedline would be moved to an RPM of 97k with about the same efficiency.

Downloaded by Gecheng Zha on February 9, 2026 | http://arc.aiaa.org | DOI: 10.2514/6.2026-0937

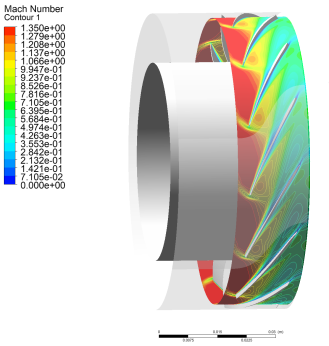

Fig. 21: Micro-compressor CFD results.

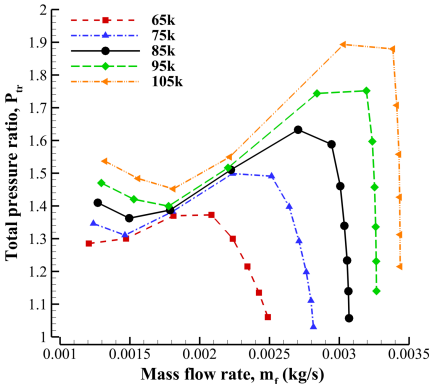

Fig. 22: Total pressure ratio vs. mass flow rate

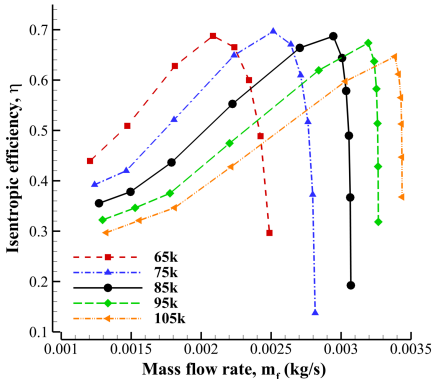

Fig. 23: Isentropic efficiency vs. mass flow rate

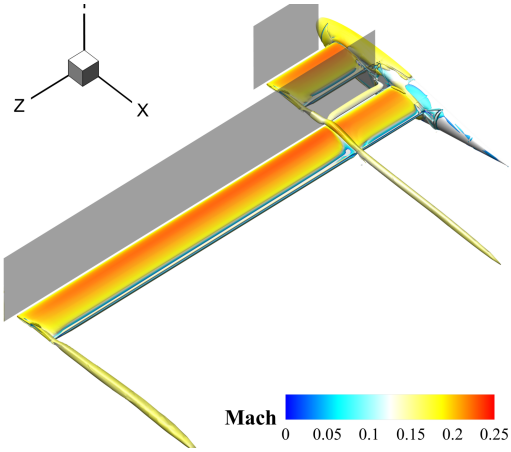

Fig. 24: Mach contours of the conventional VTOL alternative aircraft.

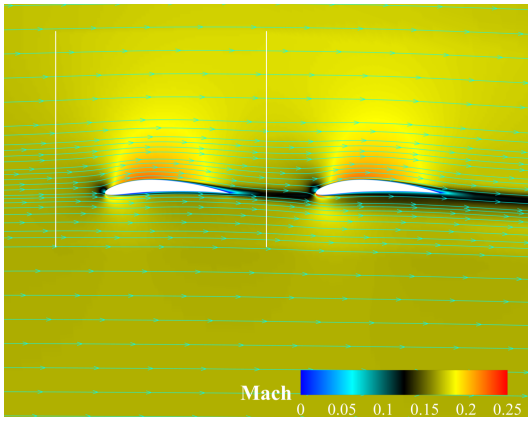

Fig. 25: Mach contours at mid-plane of canard with the main wing

8 Launch Mission from Earth to Mars

With MAGGIE's maximum wing span of 14 m and fuselage length of 4 m, there are a few rocket system that have the technological and dimensional capabilities to complete a successful Earth-to-Mars mission without folding the wings, including Vulcan Centaur, SLS Block B2, and SpaceX's Starship. Vulcan Centaur has a pay load fairing (PLF) with the dimension of 5.4 m (Diameter) × 15.5 - 21. 3 m (Height). SLS B2 has a PLF of 8.4 × 27.4 m. Both Vulcan Centaur and SLS would require MAGGIE, with its aeroshell and heat shield, to be placed vertically in the PLF. An ellipsoidal aeroshell with a deployable heat shield would be used. MAGGIE would employ an entry, descent, and landing (EDL) process similar to that of Curiosity and Perseverance to mitigate the EDL risk. The final landing on Mars surface would also use the SkyCrane process. If the SpaceX Starship rocket is used, the PLF is larger than those of the SLS rockets. The Starship is anticipated to land on Mars using supersonic retro-propulsion. The rocket would be designed to decelerate aerodynamically with the vehicle heatshield designed to withstand multiple entries, making it possible to transport MAGGIE without needing an EDL system, which can significantly decrease costs and minimize risks and potential loss of aircraft.

9 Compared with the State of the Art and the Alternatives

To facilitate the comparison, the basic equations of lift and drag for cruise, and hover power loading (power required to lift up per unit weight; PL) for a helicopter are put below for reference:

Downloaded by Gecheng Zha on February 9, 2026 | http://arc.aiaa.org | DOI: 10.2514/6.2026-0937

Table 3: Compressor geometry and operating parameters at design point.

Number of rotor blades	15
Inlet hub radius	25.4 mm
Casing radius	38.0 mm
Rotational speed	85,000 RPM
Design mass flow rate	2.9 g/s
Design total pressure ratio	1.6
Design point efficiency	70%
Power	89.9 W
Tip clearance	0.15 mm

$$L = W = \frac{1}{2}\rho V^2 C_L S, \quad D = T = \frac{1}{2}\rho V^2 C_D S, \tag{9}$$

$$PL = \sqrt{DL/2\rho} \tag{10}$$

where L, W, D and T are the lift, aircraft gross weight, drag, and propulsion thrust. Here ρ is the freestream flow density, V is the vehicle flight speed, C_L the lift coefficient, C_D the drag coefficient, S the aircraft wing planform area, and DL the disk loading at hover (lift per unit propeller disk area).

9.1 Compared with Mars Rotorcraft Chopper

Chopper is a state of the art potential VTOL aircraft for flying on Mars recently studied by NASA, JPL, Analytical Mechanics Associates, and Science and Technology Corporation [9]. It is a concept evolved from MSH [62, 75, 84]. It is feasible for performing a science mission powered by solar energy. Chopper would be able to have a payload of 3 kg and conduct science exploration with a range of 3 km per sol, about 2,000 km in a Martian year, covering a substantially larger area than the ground rovers.The altitude of Chopper's flight is not clearly given [9], but is expected to be similar to that of MSH, 200 m. In comparison, MAGGIE is designed to cruise at 1000 m, and can fly up to 12-km altitude as the service ceiling. MAGGIE could traverse 40,000+ km areas in one Martian year with a payload capacity of 20 kg to perform more sophisticated science investigations at a much larger global scale, allowing for a substantially enhanced science mission, and many more viable mission concepts (see Section 10).

9.2 Compared with the Alternative Conventional Approaches

To compare with an alternative fixed wing VTOL aircraft using a conventional airfoil, we designed an alternative aircraft (AA) that has the same configuration and size as that of MAGGIE, but using a conventional NACA6410 airfoil with no CFJ. The NACA-6410 airfoil is selected to optimize the aerodynamic efficiency and structural integrity at low *Re*. At an AoA of 4°, the AA achieves its best aerodynamic efficiency of C_L/C_D =13.55 with an excellent C_L of 0.427 based on conventional aerodynamic measure of merits. The C_L is almost an order of magnitude smaller than that of the MAGGIE, and could be further reduced if a sufficient stall margin is considered. Fig. 24 shows the 3D Mach contours of the aircraft at the same cruise conditions as given in Table 1. Fig. 25 is the 2D cross section at the same location as in Fig. 14. However, the total lift of the AA can only support a gross mass of 16.18 kg, about 13% of the mass of MAGGIE. The lift is not sufficient to support even the weight of its wings and fuselage (estimated using the same method for MAGGIE) without even considering any propulsors, solar panels, batteries, payload, etc. The AA is thus not feasible. For the same configuration, we could also scale up its size so that aerodynamically it could generate the same total lift as that of MAGGIE based on Eq. (9). In this case, the AA's wing area would be 97.6 m^2 with a wing span of 41 m. This is a very large aircraft and the weight also grows substantially. It ends up

Downloaded by Gecheng Zha on February 9, 2026 | http://arc.aiaa.org | DOI: 10.2514/6.2026-0937

having the same problem that the lift is insufficient to support its own structural weight even without any other components or payload. It has an additional problem that the size would be too large to fit into any of the rockets even with a folding of the wing structure. The alternative approaches using conventional fixed wing VTOL configurations are thus deemed infeasible.

9.3 Analysis on the Comparison

In aerodynamics, helicopter hover power loading is inversely proportional to $\sqrt{\rho}$ as indicated in Eq. (10). For the same DL, the power loading on Mars would be an order of magnitude higher than that on Earth. Since a helicopter flies forward by slightly tilting the rotor disk, the cruise power is not much smaller than that at hover. MSH has a cruise power about 80% of its hover power [62], penalizing the mission efficiency with limited range and payload. But, the proximity of lift and power between cruise and hover makes a helicopter feasible to fly on Mars.

However, things often have two sides. The low air density could also bring a very large advantage in that the cruise power for a fixed wing aircraft , $P = VD = \frac{1}{2}\rho V^3 C_D S$, could be two orders of magnitude lower than that on Earth, assuming a similar flight speed and drag coefficient. But this advantage can only be realized if the aircraft is flyable on Mars with $L = W$ for cruise as indicated in Eq. (9). Eq. (9) shows the barrier to flying a fixed wing aircraft on Mars is that the lifting capability provided by the dynamic pressure $1/2\rho V^2$ is only about 3% of that on Earth considering the gravitational acceleration effect. Eq. (9) indicates that there may be three ways to increase the total lift : 1) increase velocity, V, by flying fast. That is the approach taken by the ARES concept previously studied by NASA [4, 6, 7], which had a cruise Mach number about 0.7 and was powered by a rocket engine just for "one shot". Such a high speed rules out using self-sufficient solar energy simply because solar energy can not provide the required high power and energy density proportional to V^3 and V^2, respectively. The "one shot" mission also had a quite limited range. 2) increase the size, S, of the aircraft. Increasing the size will also increase the weight at the same time, which is difficult to be offset by the low lift on Mars as shown in the comparison above for the alternative approach. 3) increase the lift coefficient, C_L. A conventional 2D airfoil has a low lift coefficient of about 0.5 at $Re < 10^5$ for the thickness of 10-12% that is suitable for a fixed wing aircraft structure [42, 44, 61]. The best airfoil, aerodynamically, is a thin plate airfoil with a thickness of 1-3%, which can provide a C_L of about 0.85. For 3D wings, all these C_L values will drop significantly. For fixed wing VTOL aircraft with a significant mass, a thin plate airfoil is very difficult to use because of its weak structure integrity and increased weight [63].

MAGGIE would be able to take advantage of the low cruise power on Mars due to its aerodynamic breakthrough of a thick flapped CFJ airfoil that provides a high aircraft C_L of 3.24 and an excellent C_L/C_{Dc} of 5.76, enabling it to fly at a low Mach number (0.17) with a compact size and light weight. As shown in Table 1, MAGGIE's cruise power is about 10% of its hover power. The low cruise power of MAGGIE would also let the batteries work most of the time at very low C-rate to have a long life span. It also allows MAGGIE to reach a high altitude of 12 km with plenty of excess power. Comparing the productivity efficiency [59], MAGGIE's is an order of magnitude greater than Chopper or MSH. At hover, MAGGIE's power is also governed by Eq. (10) and is slightly higher than that of a helicopter due to CFJ in Mars' atmosphere, but the hover mode lasts a very short time (< 30 s) and only consumes a small amount of energy, which has little impact on the mission range as shown in Table 1. MAGGIE also efficiently integrates the solar panel as a part of the wing configuration, whereas Chopper or MSH has to carry a dedicated solar panel that interacts with the downwash of the helicopter and decreases its aerodynamic efficiency. The above features may make a solar powered Mars helicopter more suitable to having a small size, whereas MAGGIE's productivity efficiency will grow with its size.

10 Science Mission

In this study, we completed a survey of the science landscape to identify those science investigations which would be most enabled by an aerial vehicle like MAGGIE, with range and altitude capabilities exceeding existing approaches. The survey examined those science measurements made from orbit that would benefit from a lower altitude and, conversely, those measurements made from the surface

Downloaded by Gecheng Zha on February 9, 2026 | http://arc.aiaa.org | DOI: 10.2514/6.2026-0937

that would benefit from a higher vantage point. We identified four top candidate instruments for a MAGGIE science mission and obtained preliminary estimates of size, weight and power (SWaP, Table 4) to establish whether they could be integrated into the MAGGIE architecture. A concept of operations for the payload was iterated as the technical design of MAGGIE was refined. This ConOps addresses all four science objectives during each of the two observation modes (surface and airborne). With it, we have demonstrated that a viable, exciting science mission can be flown with our preferred payload in Table 4.

Instrument	Volume	Weight	Power
Magnetometer	Sensor + Electronics: 10 cm^3	0.6 kg	1 W
Ground-Penetrating Radar	Radar + Antenna: < 1 m^3	2-3 kg	2.5 W(idle) 9.5 W(sounding)
Tunable Laser Spectrometer	3 $liters$ (sensor) + 15 cm telescope, supports	2-3 kg	10-20 W
Meteorology Suite	All sensors: 10s cm^3	2-3 kg	5 W (idle) 10 W(sounding)

Table 4: Instruments Payload of Representative MAGGIE Mission

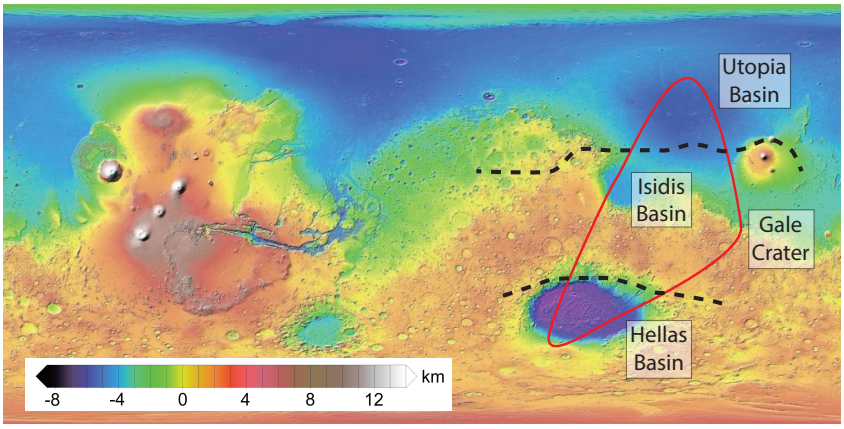

Fig. 26: Mars topographic map illustrating representative mission flight path (red loop).

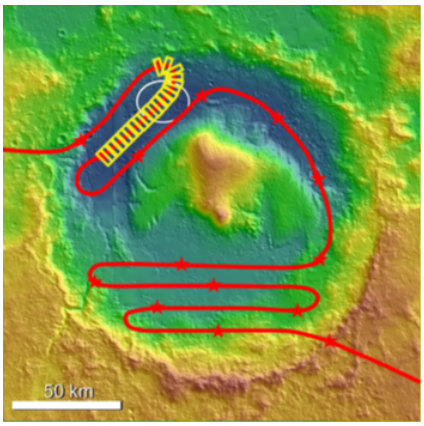

Fig. 27: Gale crater Topography and notional flight path by MAGGIE (red line), Stars: surface science with TLS and recharge; White oval: landing for MSL.

We have developed a representative mission (Fig. 26, and discussed below), which would address these four atmospheric and geophysical science objectives aligned with these community and agency scientific priorities for the robotic exploration of Mars. The representative mission (Fig. 26) would entail MAGGIE flying and landing along a regional-scale loop in the eastern hemisphere of Mars over the course of one Mars year. Investigations would be conducted both in flight and on the ground. An important innovation of MAGGIE is its ability to explore everywhere on Mars, including the southern hemisphere where landed missions are extremely challenging because of difficult entry, descent, and landing (EDL) caused by the high elevation. MAGGIE offers the ability to land in the Northern Lowlands where EDL is comparatively simpler in the lower elevation, smoother terrain and then fly to the Southern Highlands, taking advantage of MAGGIE's capability to range 1000s of km. If possible for the prospective launch window, the mission would approximately track the latitude of the Sun to maximize available solar power. Key regions of investigation for the primary representative mission include large impact basins, Gale crater, and areas in both hemispheres where near-surface water ice has been detected.

A notional payload for MAGGIE, with preliminary estimates of payload mass, power and volume, is shown in Table 4. In addition, cameras for operational use would be included to provide imagery of the

Downloaded by Gecheng Zha on February 9, 2026 | http://arc.aiaa.org | DOI: 10.2514/6.2026-0937

surrounding landscape and to assist with descent and landing activities. Because of the comparatively low power requirements of the science payload compared to requirements for flying, there are few limits on when observations could be made from MAGGIE. In future studies, we will determine the amount and precision of observations that can be taken, as discussed below. Application of these instruments towards the mission objectives is discussed presently.

10.1 Objective 1: Determine the timing of the ancient Martian core dynamo

MAGGIE provides an excellent mission architecture to study the history of the Martian core by measuring the magnetization of strategically chosen parts of the Martian crust with a magnetometer. The crustal magnetic field has been measured globally from orbit (e.g., [85,86]), but magnetic measurements taken on the ground at a single location show that the true magnitude of crustal magnetization may be very different than values derived from orbit [62]. MAGGIE would be game-changing in addressing the current gap between global but low-resolution orbital measurements and high-resolution but stationary measurements from a static lander with its aerial mobility and ability to map the magnetic field from 100s-of-m to km-scale altitudes. For example, some large impact basins on Mars appear unmagnetized or only weakly magnetized from orbit, an observation that could imply that the dynamo was inactive during the Noachian period (e.g., [85,87]) or that the dynamo was active but basins appear unmagnetized from orbit because of the way the impact process excavated material [88], or that the post-impact crust cooled during polarity reversals [89]. These competing hypotheses make different predictions for the spatial distribution of the crustal magnetic field that would be observed today as a function of altitude. Our representative mission would include data collection over the Utopia, Isidis, and Hellas basins (Fig. 26), testing these hypotheses by mapping the magnetic field over these basins. MAGGIE's ability to fly to 12 km altitude would enable these tests because magnetic fields quickly decay with distance [90].

10.2 Objective 2: Distinguish between competing hypotheses on the distribution of mid-latitude ice on Mars

Our representative science mission allows MAGGIE to test for the presence of mid-latitude ice deposits and characterize their physical properties with a ground-penetrating radar (GPR). Although we know some shallowly buried ice exists in the Martian mid-latitudes [91], most directly on the basis of its direct excavation from small impacts [92], its purity and vertical and lateral extent are debated, with different analyses yielding seemingly inconsistent results (e.g., [93,94]). Distinguishing between these competing hypotheses would elucidate the dynamics of recent Martian climate, especially in understanding the stability of non-polar ice under the planet's current orbital configuration (e.g., [95]). Our representative mission includes data collection with GPR in Utopia Planitia, one of the best candidates for mid-latitude ice and an especially promising location as the landing site of future astronauts [96]. Analyzing heterogeneity directly at these small scales is challenging from orbital radar sounding. MAGGIE would enable this investigation with its high-resolution sounding and mobility, either by operating the GPR during low altitude flight or while grounded in a regular pattern over Utopia Planitia.

10.3 Objective 3: Localize sources of methane emission identified on the martian surface

It continues to be of great interest to localize the source(s) of previously identified methane releases in/around Gale crater [97–99] because of the potential of an active methane release being indicative of biologic activity. Our representative science mission allows us to address this question by flying a high-sensitivity TLS to detect methane signals both during flight and on the surface. A notional flight path through Gale crater is shown by the red line in Fig. 27. Stars indicate points along the path approximately 50 km apart where MAGGIE would touch down to recharge and conduct surface science. Yellow rectangles indicate the approximate scale of each 1-minute TLS observation for a typical sol (Mars day). A modest-sized telescope could make methane measurements with a sensitivity of a few pptv, or about 10-100 times the sensitivity of the Mars Science Laboratory (MSL) TLS instrument [100].

Downloaded by Gecheng Zha on February 9, 2026 | http://arc.aiaa.org | DOI: 10.2514/6.2026-0937

Observations above the mixed layer (> 10 km) could address hypotheses about the diurnal ventilation of near-surface methane releases, potentially explaining the lack of detection by the ExoMars Trace Gas Orbiter. Here, the MAGGIE TLS benefits from the long path length introduced by the airplane's altitude, yielding a path length more than two orders of magnitude longer than its MSL counterpart [97].

10.4 Objective 4: Characterize dynamics of the martian lower atmosphere

A small and lightweight meteorology payload can be installed on MAGGIE to conduct measurements both during flight and while on the surface directly measuring, for the first time, atmospheric properties throughout the near-surface boundary layer. Our representative mission enables MAGGIE to conduct measurements during flight, as well as while landed, obtaining atmospheric data both near the surface and at altitudes as high as 12 km, where data have never previously been acquired. A baseline suite would consist of pressure and temperature sensors, along with a selection of radiation sensors to measure downwelling radiation. Such instruments can be operated both during flight and on the surface. Additional instrumentation can be employed most effectively in one or the other operating mode. Downward-looking radiation sensors can be operated on the ground to detect upwelling surface radiation (both visible and infrared) for measuring surface properties and ground temperature. An upward looking visible camera can measure atmospheric opacity and cloud cover. While in flight, a deployed wind sensor can be used to determine boundary layer wind speed and direction free of the influence of the martian surface. Vertical ascent to 12 km would traverse the full boundary layer, and distinguish atmospheric conditions in the mixed layer from those in the free atmosphere.

11 Potential Impact

Just as the Ingenuity helicopter generated national excitement with the notion of flying on another planet, the potential for similar enthusiasm for a long-duration flyer is high. MAGGIE will, for the first time, study the rocky, ancient Southern Highlands an area of immense scientific value, but also of great public engagement potential. From its vantage point 1 kilometers above the surface, MAGGIE will acquire sweeping views of the surrounding vistas, providing a wealth of exciting visuals for both the science community as well as the public, all while addressing some of the most important science questions of the Mars community. MAGGIE also introduces a new way of accessing this heretofore unexplored region of the planet. With its exceptional range, MAGGIE can leverage the benefits of landing in the Northern Lowlands, before taking off, flying south, and ascending the dichotomy boundary, all the while acquiring new and valuable scientific data about the surface and near surface geophysical environment. Alternative approaches for landing in the southern hemisphere include hard impact of a landed payload or mid-air deployment of an aerial vehicle. In both cases, payload size is limited, and spacecraft range is comparatively small (or nonexistent). Alternatively, MAGGIE offers the potential to conduct a wide-ranging reconnaissance survey of unexplored terrain while simultaneously allowing targeted science in regions of interest.

CFJ achieves an aerodynamic technology breakthrough at the airfoil level, which is the most fundamental element of all lifting devices. The technology developed for MAGGIE thus can benefit many fluid machinery applications. The MAGGIE technology could be potentially used for manned or unmanned aerial transportation vehicles for future Mars colonization due to its unique ultra-high lift and productivity efficiency. MAGGIE technology could be also used for exploration of other planets with atmospheres such as Venus and Jupiter.

12 Conclusions

This study indicates that the MAGGIE concept and mission are feasible at the conceptual design level. MAGGIE is a compact fixed wing aircraft with ultra-high productivity efficiency powered by solar energy to fly in the Martian atmosphere. It has vertical take-off/landing (VTOL) capability enabled by advanced deflected slipstream CoFlow Jet (CFJ) technology. MAGGIE is designed to have a gross weight of 125 kg, payload of 20 kg, wing span of 14.12 m, and a total range of 42,011 km with level cruise for a one Martian year mission. It cruises at a Mach number of 0.17 at an altitude of 1000 m

Downloaded by Gecheng Zha on February 9, 2026 | http://arc.aiaa.org | DOI: 10.2514/6.2026-0937

with the service ceiling of 12 km. CoFlow Jet (CFJ) Active Flow Control (AFC) would be the enabling technology to operate in Mars' low Reynolds number ($Re < 10^5$) conditions with an ultra-high cruise lift coefficient of $C_L = 3.24$ and aerodynamic efficiency of 5.76. The critical hover-cruise transition enabled by deflected slipstream with CFJ in the Martian condition is proven to be achievable by a preliminary 2D unsteady simulation. It is also proven feasible to design a micro-compressor actuator to fit inside of the CFJ-NACA6421 airfoil with a high efficiency of 70% in Mars' low *Re* conditions. Rocket launch and EDL (entry, descent, landing) for MAGGIE are feasible by using Vulcan Centaur, NASA's SLS (B2), or SpaceX Starship.

There are three types of flight trajectories for MAGGIE based on the science missions: 1) Level Cruise: cruise at 1000 m altitude for a range of 125.8 km per charge, suitable for meteorology or ice measurements; 2) Climb-and-Glide: climb to service ceiling of 12 km and then glide to ground for the longest range of 139.84 km per charge, useful for long range flight to the regions where EDL is challenging, like the southern highlands; 3) Climb-and-Spiraling Glide: climb to the service ceiling above the location of interest and then descend via spiral-glide, suitable for magnetic field measurements. All three trajectories can incorporate "scout-and-land" flight missions.

Based on the survey of the science landscape conducted in this study, a potentially ground breaking representative mission enabled by the long range and high payload capacity of MAGGIE is developed to address four atmospheric and geophysical science objectives: 1) Determine the timing of the ancient Martian core dynamo; 2) Distinguish between competing hypotheses on the distribution of mid-latitude ice on Mars; 3) Localize sources of methane emission identified on the martian surface; 4) Characterize dynamics of the martian lower atmosphere.

Compared with the state of the art Mars Rotorcraft Chopper, which would have a payload of 3 kg, a range of 3 km per sol that would translate to a range of 2,000 km per Martian year, MAGGIE would span 40,000+ km areas per year with a payload of 20 kg, a cruise altitude of 1000 m, and a service ceiling of 12,000 m to perform global scale, advanced science investigations in the atmosphere and on the ground.

For comparison, an alternative aircraft (AA) using a conventional 10% thickness airfoil for a fixed wing eVTOL is designed with the same configuration as MAGGIE. The AA achieves excellent aerodynamic performance based on conventional criteria. However, the lift of the AA is not able to lift up its own structure weight on Mars. The alternative approaches are thus deemed infeasible.

MAGGIE would be the first mission to enable widespread exploration of the ancient southern highlands of Mars and would provide a substantial leap in capability for NASA's exploration of the Red Planet. The same technology can be used to design transportation vehicles on Mars for future manned mission and colonization. It can be also used to enhance the efficiency of VTOL aircraft on Earth.

Downloaded by Gecheng Zha on February 9, 2026 | http://arc.aiaa.org | DOI: 10.2514/6.2026-0937

13 Acknowledgment

This project is sponsored by NASA NIAC Grant Number 80NSSC24K0647. The numerical simulation of MAGGIE vehicle design and analysis and science missions is conducted with the computing resource of NASA High-End Computing systems. We greatly appreciate all the support from NASA. A portion of this work was conducted at the Jet Propulsion Laboratory, California Institute of Technology, under contract with NASA.

References

[1] National Research Council, "Scientific Rationale for Mobility in Planetary Environments." Committee on Planetary and Lunar Exploration Space Studies Board, Commission on Physical Sciences, Mathematics, and Applications, 1999.

[2] "MEPAG MCE-SAG Final Report, Chaired by M. Mischna and B. Horgan, 94pp. Posted on 18 July 2023 by the Mars Exploration Program Analysis Group at: https://www.lpi.usra.edu/mepag/report/reports/MCE_SAG_Final_Report.pdf," *Mars Concurrent Exploration Science Analysis Group (MCE-SAG)*, 2023.

[3] "Exploring Mars Together: A plan for a sustainable future for science at Mars,

https://mars.nasa.gov/files/mep/ Mars_Exploration_Program_Future_Plan.pdf," *Mars Exploration Program (MEP)*, 2023.

[4] Guynn, M. D. and Croom, M.A. and Smith, S. C. and Parks, R. W. and Gelhausen, R. W., "Evolution of a Mars Airplane Concept for the ARES Mars Scout Mission ." AIAA Paper 2003-6578, Sept. 2003.

[5] Sandford, S.P. et al., "Ares and beyond: Autonomous aerial platforms provide a unique measurement capability for earth and planetary science," in *2nd AIAA" Unmanned Unlimited" Conf. and Workshop & Exhibit*, p. 6610, 2003.

[6] Levine, J.S. et al., "Science from a mars airplane: The aerial regional-scale environmental survey (ARES) of mars," in *2nd AIAA" Unmanned Unlimited" Conf. and Workshop & Exhibit*, p. 6576, 2003.

[7] Levine, J.S. et al., "The Aerial Regional-scale Environmental Survey (ARES): A New Tool for the Exploration of Mars," in *37th Annual Lunar and Planetary Science Conference*, p. 1311, 2006.

[8] Y. Wang and G.-C. Zha, "Study of Reynolds Number Effect for 2D Co-Flow Jet Airfoil at Cruise Conditions." AIAA-2020-2666, AIAA Aviation Virtual Forum, 15-19 June, 2020.

[9] S. Withrow-Maser, W. Johnson, W. Koning, and et al, "Critical aerodynamic and performance upgrades to enable larger Mars rotorcraft such as the chopper platform." Proceedings of Vertical Flight Society's 81st Annual Forum & Technology Display, Virginia Beach, VA, USA, May 20-22, 2025.

[10] Bapst, J. et al., "Mars science helicopter: Compelling science enabled by an aerial platform." White paper submitted to Planetary Science and Astrobiology Decadal Survey, 2021.

[11] C. Dull, L. Wagner, L. Young, and W. Johnson, "Hover and Forward Flight Performance Modeling of the Ingenuity Mars Helicopter." VFS Aeromechanics for Advanced Vertical Flight Technical Meeting, San Jose, CA, Jan 25-27, 2022.

[12] V. V.Kenhanovich and J. A.Cutt, "RECENT PROGRESS IN PLANETARY BALLOONS ." 15th ESA Symposium on European Rocket and Balloon Programmes and Related Research, Biarritz, France. Ed.: Barbara Warmbein. ESA SP-471, Noordwijk: ESA Publications Division, ISBN 92-9092-725-9, 2001, p. 647 - 652, 28 - 31 May 2001.

[13] X. Chen and G.-C. Zha, "Implicit Application of Non-Reflective Boundary Conditions for Navier-Stokes Equations in Generalized Coordinates," *International Journal for Numerical Methods in Fluids*, vol. 50, 2006.

[14] Shen, Y.-Q. and Zha, G.-C. and Chen, X.-Y., " High Order Conservative Differencing for Viscous Terms and the Application to Vortex-Induced Vibration Flows," *Journal of Computational Physics*, vol. 228(2), pp. 8283–8300, 2009.

[15] Y.-Q. Shen and G.-C. Zha, "Large Eddy Simulation Using a New Set of Sixth Order Schemes for Compressible Viscous Terms ," *Journal of Computational Physics*, vol. 229, pp. 8296–8312, 2010.

[16] Shen, Y.-Q. and Zha, G.-C. and Wang, B.-Y., " Improvement of Stability and Accuracy of Implicit WENO Scheme," *AIAA Journal*, vol. 47, No. 2, pp. 331–344, 2009.

[17] Shen, Y.-Q. and Zha, G.-C. , " Improvement of the WENO Scheme Smoothness Estimator," *International Journal for Numerical Methods in Fluids*, vol. 64, p. DOI:10.1002/fld.2186, 2010.

[18] Shen, Y.-Q. and Zha, G.-C., " Improved Seventh-Order WENO Scheme ." AIAA Paper 2010-1451, 48th AIAA Aerospace Sciences Meeting, Orlando, FL, Jan. 4-6, 2010.

[19] Y.-Q. Shen and G.-Z. Zha , "Generalized finite compact difference scheme for shock/complex flowfield interaction," *Journal of Computational Physics*, vol. doi:10.1016/j.jcp.2011.01.039, 2011.

[20] G.-C. Zha, Y. Shen, and B. Wang, "An improved low diffusion E-CUSP upwind scheme ," *Journal of Computer & Fluids*, vol. 48, pp. 214–220, 2011.

[21] B.-Y. Wang and G.-C. Zha, "A General Sub-Domain Boundary Mapping Procedure For Structured Grid CFD Parallel Computation," *AIAA Journal of Aerospace Computing, Information, and Communication*, vol. 5, No.11, pp. 2084–2091, 2008.

[22] Im, H.-S. and Zha, G.-C. and Dano, B. P. E., "Large Eddy Simulation of Coflow Jet Airfoil at High Angle of Attack," *Journal of Fluid Engineering*, vol. 136(2), p. 021101, 2014.

Downloaded by Gecheng Zha on February 9, 2026 | http://arc.aiaa.org | DOI: 10.2514/6.2026-0937

[23] Wang, B. Y and Zha, G.-C., "High Fidelity Simulation of Nonlinear Fluid-Structural Interaction with Transonic Airfoil Limit Cycle Oscillations," *Journal of Fluids and Structures*, vol. doi:10.1016/j.jfluidstructs.2010.02.003, 2010.

[24] Lefebvre, A. and Dano, B. and Bartow, W. and Di Franzo, M. and Zha, G.-C., "Performance and Energy Expenditure of Co-Flow Jet Airfoil with Variation of Mach Number," *AIAA Journal of Aircraft*, vol. 53, pp. 1757–1767, 2016.

[25] Xu, Kewei and Zha, Gecheng, "Enhancing aircraft control surface effectiveness by co-flow jet flap at low energy expenditure ," *Elsevier Journal of Aerospace Science and Technology*, vol. 133, 2023.

[26] Y. Wang and G.-C. Zha, "Study of Mach Number Effect for 2D Co-Flow Jet Airfoil at Cruise Conditions." AIAA Paper 2019-3169, AIAA Aviation 2019, AIAA Applied Aerodynamics Conference, Dallas, Texas, 17-21 June 2019.

[27] Y. Wang, Y.-C. Yang, and G.-C. Zha, "Study of Super-Lift Coefficient of Co-Flow Jet Airfoil and Its Power Consumption." AIAA Paper 2019-3652, AIAA Aviation 2019, AIAA Applied Aerodynamics Conference, Dallas, Texas, 17-21 June 2019.

[28] Y. Wang and G.-C. Zha, "Study of 3D Co-flow Jet Wing Induced Drag and Power Consumption at Cruise Conditions." AIAA Paper 2019-0034, AIAA SciTech 2019, San Diego, CA, January 7-11, 2019.

[29] P. Roe, "Approximate Riemann Solvers, Parameter Vectors, and Difference Schemes," *Journal of Computational Physics*, vol. 43, pp. 357–372, 1981.

[30] G. C. Zha, D. Smith, M. Schwabacher, K. Rasheed, A. Gelsey, and D. Knight, "High Performance Supersonic Missile Inlet Design Using Automated Optimization." AIAA Paper 96-4142, 1996.

[31] Zha, G.-C. and Gao, W. and Paxton, C., "Jet Effects on Co-Flow Jet Airfoil Performance," *AIAA Journal, No. 6,*, vol. 45, pp. 1222–1231, 2007.

[32] Zha, G.-C and Carroll, B. and Paxton, C. and Conley, A. and Wells, A., "High Performance Airfoil with Co-Flow Jet Flow Control," *AIAA Journal*, vol. 45, 2007.

[33] Zha, G.-C and Paxton, C. and Conley, A. and Wells, A. and Carroll, B., "Effect of Injection Slot Size on High Performance Co-Flow Jet Airfoil," *AIAA Journal of Aircraft*, vol. 43, 2006.

[34] Wang, B.-Y. and Haddoukessouni, B. and Levy, J. and Zha, G.-C., "Numerical Investigations of Injection Slot Size Effect on the Performance of Co-Flow Jet Airfoil ," *AIAA Journal of Aircraft*, vol. 45, pp. 2084–2091, 2008.

[35] Wang, B. Y and Zha, G.-C., " Detached-Eddy Simulation of a Co-Flow Jet Airfoil at High Angle of Attack ," *AIAA Journal of Aircraft*, vol. 48, pp. 1495–1502, 2011.

[36] Liu, Z.-X. and Zha, G.-C., "Transonic Airfoil Performance Enhancement Using Co-Flow Jet Active Flow Control." AIAA Paper 2016-3472, AIAA AVIATION 2016, 8th AIAA Flow Control Conference, Washington, D.C, June 13-17, 2016.

[37] Yang, Y.-C. and Fernandez, M. and Zha, G.-C., "Improved Delayed Detached Eddy Simulation of Super-Lift Flow of Co-Flow Jet Airfoil." AIAA Paper 2018-0314, AIAA SciTech Forum, 2018 AIAA Aerospace Sciences Meeting, Kissimmee, FL, 8-12 January 2018.

[38] Yang, Y.-C. and Zha, G.-C., "Super Lift Coefficient of Cylinder Using Co-Flow Jet Active Flow Control." AIAA Paper 2018-0329, AIAA SciTech Forum, 2018 AIAA Aerospace Sciences Meeting, Kissimmee, FL, 8-12 January 2018.

[39] D. Espinal, H.-S. Im, and G.-C. Zha, "Full-annulus simulation of nonsynchronous blade vibration excitation of an axial compressor," *Journal of Turbomachinery*, vol. 140, pp. 031008–1, 2018.

[40] Y.-C. Yang, W. B. Bartow, G.-C. Zha, H.-Y. Xu, and J.-L. Wang, "Large eddy simulation of base drag reduction using jet boat tail passive flow control," *Journal of Computers and Fluids*, vol. 198, Feb. 2020.

[41] B. Wang and G. - C. Zha , " Detached Eddy Simulations of a Circular Cylinder Using a Low Diffusion E-CUSP and High-Order WENO Scheme." AIAA Paper 2008-3855, AIAA 38th Fluid Dynamics Conference, Seattle, Washington, June 23-26, 2008.

[42] W. J. F. Koning, W. Johnson, and H. F. Grip, "Improved mars helicopter aerodynamic rotor model for comprehensive analyses," *AIAA Journal*, vol. 57 (9), p. 982993, 2019.

Downloaded by Gecheng Zha on February 9, 2026 | http://arc.aiaa.org | DOI: 10.2514/6.2026-0937

[43] W. J. F. Koning, W. Johnson, and B. G. Allan, "Generation of mars helicopter rotor model for comprehensive analyses," in *AHS Aeromechanics Design for Transformative Vertical Flight, American Helicopter Soc. (AHS) SKU: sm-aeromech-2018-17,*, (Fairfax, VA), 2018.

[44] J. Winslow, H. Otsuka, B. Govindarajan, and I. Chopra, "Basic understanding of airfoil characteristics at low reynolds numbers," *Journal of Aircraft*, vol. 55 (3), pp. 1050–1061, 2018.

[45] C. L. Rumsey and P. R. Spalart, "Turbulence model behavior in low reynolds number regions of aerodynamic flowfields," *AIAA Journal*, vol. 47 (4), p. 982993, 2009.

[46] G.-C. Zha, Y. Ren, M. Anhalzer, M. A. Mischna, and M. M. Sori, "Mars Aerial and Ground Global Intelligent Explorer (MAGGIE) ." Final Report submitted to NASA NIAC Phase I program, Grant Number 80NSSC24K0647, Feb. 2025.

[47] W. J. F. Koning, E. A. Romander, and W. Johnson, "Performance optimization of plate airfoils for martian rotor applications using a genetic algorithm," in *Presented at the 45th European Rotorcraft Forum*, (Warsaw, Poland), 17-20 September, 2019.

[48] Phillip M. Munday, Kunihiko Taira, Tetsuya Suwa, Daiju Numata and Keisuke Asai, "Nonlinear Lift on a Triangular Airfoil in Low-Reynolds-Number Compressible Flow," *Journal of Aircraft, Volume 52, Number 3, Dec 2014*, 2014.

[49] Zha, G.-C. and Ren, Y. and Fredericks, W. , "Design and Testing of Deflected Slipstream Airfoil for VTOL Hover Enabled by CoFlow Jet." AIAA Paper 2024-4420, AIAA AVIATION FORUM AND ASCEND 2024, Las Vegas, Nevada, 29 July - 2 August 2024.

[50] G.-C. Zha, "Feasibility Study of Deflected Slipstream Airfoil for VTOL Hover Enabled by CoFlow Jet." AIAA Paper 2023-4279, AIAA Aviation Forum 2023, San Diego, CA, 12-16 June 2023.

[51] G.-C. Zha, "Design and Support for CoFlow Jet Experiment for Deflected Slipstream." Final Report to NASA, Subcontract No: T16-6500-CJL, Task Order No. 602005, Prime Contract NNL13AA08B, June 2023.

[52] R. E. Kuhn and J. W. Draper, "An Investigation of a Wing-Propeller configuration Employing Large-Chord Plain Flaps and Large-Diameter Propellers for Low-Speed Flight and Vertical Take-Off ." NACA TN-3307, December 1954.

[53] R. E. Kuhn and J. W. Draper, "Investigation of Effectiveness of Large-Chord Slotted Flaps in Deflecting Propeller Slipstreams Downward for Vertical Take-Off and Low-Speed Flight ." NACA TN-3364, Jan. 1955.

[54] K. R. Antcliff, S. K. Whireside, L. W. Kohlman, and C. Silva, "Baseline Assumptions and Future Research Areas for Urban Air Mobility Vehicles." AIAA Paper 2019-0528, AIAA SciTech 2019 Forum, San Diego, CA, 7-11 January 2019.

[55] Y. Ren and G.-C. Zha, "Design and analysis of tandem wing aircraft at ultra-low Reynolds numbers in cruise condition." AIAA Paper 2025-3639, AIAA AVIATION FORUM AND ASCEND 2025, Las Vegas, Nevada, 21 - 25 July 2025.

[56] Y. Ren and G.-C. Zha, "Performance enhancement by tandem wings interaction of coflow jet aircraft." AIAA-2021-1823, AIAA SciTech Forum 2021, Virtual Event, 1115, 1921 January 2021,.

[57] J. Boling and G.-C. Zha, " Numerical Investigation of Longitudinal Static Stability of a High-Speed Tandem-Wing VTOL Vehicle Using CoFlow Jet Airfoil." AIAA Paper 2021-1732, 2021 AIAA SciTech Virtual Forum, 15-19 June, 2020.

[58] B. McBreen and J. Boling and Y. Ren and and G.-C. Zha, "Variation of Moments for a Tailless High-Speed Tandem Wing VTOL Aircraft Using Distributed Propulsors and CoFlow Jets." AIAA Paper 2023-4282, AIAA AVIATION 2023 Forum, San Diego, CA, 12-16 June 2023.

[59] Yang, Y.-C. and Zha, G.-C., "Super-Lift Coefficient of Active Flow Control Airfoil: What Is the Limit?." AIAA Paper 2017-1693, AIAA SCITECH2017, 55th AIAA Aerospace Science Meeting, Grapevine, Texas, 9-13 January 2017.

[60] G.-C. Zha, Y.-C. Yang, Y. Ren, and B. McBreen, "Super-lift and thrusting airfoil of coflow jet-actuated by micro-compressors." AIAA Paper 2018-3061, AIAA AVIATION 2018, Atlanta, GA , 25 - 29 June 2018.

[61] S. F. Hoerner, *Fluid-Dynamic Drag.* Midland Park, NJ: Hoerner Fluid Dynamics, 1965.

Downloaded by Gecheng Zha on February 9, 2026 | http://arc.aiaa.org | DOI: 10.2514/6.2026-0937

[62] Johnson, W. and Withrow-Maser, S. and Young, L. and Malpica, C. and Koning, W. J.F. and Kuang, W. and Fehler, M. and Tuano, A. and Chan, A. and Datta, A. and Chi, C. and Lumba, R. and Escobar, D. and Balaram, J. and Tzanetos, T. and Grip, H. F., "Mars Science Helicopter Conceptual Design." NASA TM2020220485, March 2020.

[63] Corke, T. C., *Design of Aircraft*. Prentice Hall, 2003.

[64] McBreen, B. and Yang, Y.-C. and Zha, G.-C., "Improved Delayed Detached Eddy Simulation of Co-Flow Jet Flow Control in Extreme Adverse Pressure Gradients." AIAA Paper 2024-0063, 2024 AIAA SciTech Forum, Orlando, FL, 8 - 12 January 2024.

[65] McBreen, B. and Butler, E. and Zha, G.-C., "Analysis of CoFlow Wall Jet in Extreme Adverse Pressure Gradient with Super-Lift Coefficient." AIAA Paper 2024-0492, 2024 AIAA SciTech Forum, Orlando, FL, 8 - 12 January 2024.

[66] McBreen, B. and Yang, Y.-C. and Zha, G.-C., "Improved Delayed Detached Eddy Simulation of Co-Flow Jet Flow Control with Enthalpy Effects." AIAA Paper 2024-3793, AIAA AVIATION FORUM AND ASCEND 2024, , 29 July - 2 August 2024.

[67] McBreen, B. and Xu, K.-W. and Zha, G.-C., "Numerical Study of Extreme Adverse Pressure gradients Enabled by Co-Flow Jet." AIAA Paper 2023-1430, AIAA 2023 SciTech Forum, National Harbor, MD , 23-27 Jan. 2023.

[68] K.-W. Xu, Y. Ren, and G.-C. Zha, "Flow separation control by coflow wall jet." AIAA Paper 2021-2946, AIAA Aviation 2021, Virtual Events, 2-6 Aug. 2021.

[69] Xu, Kewei and Ren, Yan and Zha, Gecheng, "Numerical Analysis of Energy Expenditure for Co-Flow Wall Jet Separation Control ," *AIAA Journal*, vol. 60, no. 5, p. doi.org/10.2514/1.J061015, 2022.

[70] Lefebvre, A. and Zha, G.-C. , "Design of High Wing Loading Compact Electric Airplane Utilizing Co-Flow Jet Flow Control." AIAA Paper 2015-0772, AIAA SciTech2015: 53rd Aerospace Sciences Meeting, Kissimmee, FL, 5-9 Jan 2015.

[71] G.-C. Zha, Y. Ren, J.-Y. Gan, and D. Espinal, "A High Efficiency Low Noise VTOL/ESTOL Concept Using CoFLow Jet Airfoil." AIAA Paper 2019-4467, AIAA Propulsion and Energy 2019 Forum, Indianapolis, Indiana, 19-22 August 2019.

[72] Y. Ren and G.-C. Zha, "High efficiency propeller-coflow jet airfoil in cruise." AIAA Paper 2020-0787, 2020 AIAA SciTech Forum, Orlando, FL, 6-10 January, 2020.

[73] Y. Ren and G.-C. Zha, "High efficiency tandem propeller-coflow jet airfoil system in cruise." AIAA-2020-2779, 2020 AIAA AVIATION Virtual Forum, 15-19 June, 2020.

[74] Jeon, Jaehyoung and Ren, Yan and Zha, Gecheng , "Flapped CoFlow Jet Wing for High Lift Cruise in the Martian Atmosphere." AIAA Paper 2024-3589, AIAA AVIATION FORUM AND ASCEND 2024 , Las Vegas, Nevada , 29 July - 2 August 2024.

[75] Pipenberg, B. T. and Keennon, M. T. and Tyler, J. D. and Langberg, S. A. and Hibbs, B. , "Design and Fabrication of the Mars Helicopter Rotor, Airframe, and Landing Gear Systems." AIAA Paper 2019-0620, AIAA Scitech 2019 Forum , San Diego, CA, 7-11 January 2019.

[76] Zha, G.-C., "Fluid Systems That Include a Co-Flow Jet." Patent US 10,106,246 B2, USPTO, Oct. 23, 2018.

[77] Y. Ren and G.-C. Zha, "2d fluid-body interaction simulation of coflow jet deflected slipstream vtol transition flight." AIAA Paper 2024-4419, AIAA AVIATION FORUM AND ASCEND 2024, Las Vegas, Nevada, 29 July - 2 August 2024.

[78] Barrios, P. A. and Ren, Y. and Zha, G.-C., "Simulation of 3D Co-Flow Jet Airfoil Control with Micro-Compressor Actuator at High Angles of Attack." AIAA Paper-2023-4208, AIAA AVIATION 2023 Forum, San Diego, CA , 12-16 June 2023.

[79] Barrios, P. A. and Ren, Y. and Zha, G.-C., "Simulation of 3D Co-Flow Jet Airfoil with Integrated Micro-Compressor Actuator at Different Cruise Mach Numbers." AIAA Paper 2023-2118, 2023 AIAA SciTech Forum, National Harbor, MD, Jan. 23-27, 2023.

[80] K.-W. Xu, B. McBreen, Y. Ren, and G.-C. Zha, "Analysis of Micro-compressor Performance with Integrated Co-flow Jet Airfoil Ducting System ." AIAA Paper 2020-0047, 2020 AIAA SciTech Forumm, Orlando, FL, 6-10 January, 2020.

Downloaded by Gecheng Zha on February 9, 2026 | http://arc.aiaa.org | DOI: 10.2514/6.2026-0937

[81] K. Xu and G. Zha, "Design of high specific speed mixed flow micro-compressor for co-flow jet actuators." ASME Paper GT-2019-90980, ASME IGTI Turbo Expo 2019, Phoenix, Arizona, USA, June 17 - 21, 2019.

[82] P. Patel and G. Zha, "Investigation of mixed micro-compressor casing treatment using non-matching mesh interface." ASME Paper GT-2019-90977, ASME IGTI Turbo Expo 2019, Phoenix, Arizona, USA, June 17 - 21, 2019.

[83] K.-W. Xu and G.-C. Zha, "Study of axial groove casing treatment for co-flow jet micro-compressor actuators." AIAA Paper 2021-1560, 2021 AIAA SciTech Virtual Forum, 11-15 January, 2021.

[84] J. e. a. Bapst, "Mars science helicopter: Compelling science enabled by an aerial platform," *Bull. Am. Astron. Soc.*, vol. 53 (4), pp. e–id 361, 2022.

[85] Acuna, M.H. et al., "Global distribution of crustal magnetization discovered by the Mars Global Surveyor MAGER experiment," *Science*, vol. 284, p. 790793, 1999.

[86] Langlais, B. et al., "A new model of the crustal magnetic field of Mars using MGS and MAVEN," *Journal of Geophysical Research: Planets*, vol. 124, no. 6, pp. 1542–1569, 2019.

[87] Lillis, R.J. et al., "Time history of the Martian dynamo from crater magnetic field analysis," *Journal of Geophysical Research: Planets*, vol. 118, no. 7, pp. 1488–1511, 2013.

[88] Mittelholz, A. et al., "Timing of the martian dynamo: New constraints for a core field 4.5 and 3.7 Ga ago," *Science Advances*, vol. 6, no. 18, p. eaba0513, 2020.

[89] Steele, S.C. et al., "Paleomagnetic evidence for a long-lived, potentially reversing martian dynamo at˜ 3.9 Ga," *Science Advances*, vol. 9, no. 21, p. eade9071, 2023.

[90] S. Steele, R. Fu, A. Mittelholz, A. Ermakov, R. Citron, and R. Lillis, " Weak magnetism of Martian impact basins may reflect cooling in a reversing dynamo ," *Nature Comm*, vol. 15, 2024.

[91] Morgan, G.A. et al., "Availability of subsurface water-ice resources in the northern mid-latitudes of Mars," *Nature Astronomy*, vol. 5, no. 3, pp. 230–236, 2021.

[92] Byrne, S. et al., "Distribution of mid-latitude ground ice on Mars from new impact craters," *science*, vol. 325, no. 5948, pp. 1674–1676, 2009.

[93] Bramson, A.M. et al., "Widespread excess ice in arcadia planitia, Mars," *Geophysical Research Letters*, vol. 42, no. 16, pp. 6566–6574, 2015.

[94] Campbell, B.A., and G.A. Morgan, "Fine-scale layering of Mars polar deposits and signatures of ice content in nonpolar material from multiband SHARAD data processing," *Geophysical Research Letters*, vol. 45, no. 4, pp. 1759–1766, 2018.

[95] A. Bramson *et al.*, "Preservation of midlatitude ice sheets on mars," *Journal of Geophysical Research: Planets*, vol. 122, pp. 2250–2266, 2017.

[96] C. Stuurman *et al.*, "Sharad detection and characterization of subsurface water ice deposits in utopia planitia, mars," *Geophysical Research Letters*, vol. 43, pp. 9484–9491, 2016.

[97] Webster, C.R. et al., "Mars methane detection and variability at Gale crater," *Science*, vol. 347, no. 6220, pp. 415–417, 2015.

[98] Webster, C.R. et al., "Background levels of methane in Mars atmosphere show strong seasonal variations," *Science*, vol. 360, no. 6393, pp. 1093–1096, 2018.

[99] Webster, C.R. et al., "Day-night differences in Mars methane suggest nighttime containment at Gale crater," *Astronomy & Astrophysics*, vol. 650, p. A166, 2021.

[100] C. R. Webster and et al., "Laboratory simulation of tunable diode laser remote measurement of atmospheric gases using topographic targets," *Applied Optics*, vol. 22, pp. 1952–1954, 1983.

Downloaded by Gecheng Zha on February 9, 2026 | http://arc.aiaa.org | DOI: 10.2514/6.2026-0937